Pergamon

PII: S0148-9062(97)00330-6

Int. J. Rock Mech. Min. Sci. Vol. 35, No. 2, pp. 195–218, 1998

Printed in Great Britain
0148-9062/98 $19.00 + 0.00

Fracture Mechanics Analysis of Cracked Discs of Anisotropic Rock Using the Boundary Element Method

CHAO-SHI CHEN
ERNIAN PAN
BERNARD AMADEI

This paper is the second of a series of two papers dealing with the determination of the deformability, tensile strength and fracturing of anisotropic rocks by diametral compression (Brazilian test) of discs of rock. It is shown how a new formulation of the Boundary Element Method (BEM), proposed recently by the authors, can be used to determine the stress intensity factors (SIFs) and the fracture toughness of anisotropic rocks from the results of diametral compression tests on initially cracked discs. Crack initiation angles and propagation paths can also be predicted using a numerical procedure based on the BEM and maximum tensile stress criterion. Numerical examples of calculation of mixed mode SIFs are presented for both isotropic and anisotropic media. The calculated SIFs for the special isotropic case are found to be in good agreement with those reported by previous authors. Diametral loading tests were conducted on Cracked Straight Through Brazilian Disc (CSTBD) specimens of a shale in order to evaluate its fracture toughness, the angle of crack initiation and the path of crack propagation. It was found that the numerical simulations of crack initiation and propagation in the CSTBD specimens of the shale were in good agreement with the experimental observations. © 1998 *Elsevier Science Ltd.*

INTRODUCTION

Fracture mechanics has been suggested as a possible tool for solving a variety of rock engineering problems, such as rock cutting, hydrofracturing, explosive fracturing, rock stability, etc. Rock (linear elastic) fracture mechanics is essentially based on the extension of Griffith theory [1] and Irwin's modification [2] to that theory which recognizes the importance of stress intensity near a crack tip. Irwin [2] introduced parameters, called *Stress Intensity Factors* (SIFs), to express the stress and displacement field near a crack tip. In general, three SIFs, called K_{I}, K_{II} and K_{III} are introduced corresponding to three basic fracture modes, e.g. mode I (opening mode), mode II (sliding mode) and mode III (tearing mode), respectively. A superposition of the three modes describes the general case of loading (mixed mode loading). For a given cracked body under a certain type of loading, the SIFs are known and the stresses and displacements near the crack tip can accordingly be determined. Hence, the problem of linear elastic fracture mechanics reduces to the determination of the crack tip SIFs.

Various methods of determination of the SIF for cracked Brazilian discs under pure mode I have been proposed in the literature. Libatskii and Kovchik [3] used an approximate integral solution, Rooke and Tweed [4] used a Fredholm equation, Isida [5] used the boundary collocation method, Murakami [6] used the finite element method and Guo *et al.* [7] used an analytical expression to an infinite cracked plate. By varying the orientation of the crack relative to the loading direction, Awaji and Sato [8] investigated the mixed mode (I–II) crack problem using the dislocation method and the boundary collocation procedure. Atkinson *et al.* [9] used a distributed dislocation method and Fowell and Xu [10] used the dislocation method combined with a superimposition technique. All the above references concur that the Brazilian disc geometry has some major advantages over other methods currently used in rock fracture tests, i.e., simpler specimen preparation, higher failure load and easier testing procedure. However, all the methods of analysis mentioned above are limited to isotropic media. Recently, Chen *et al.* [11] proposed a method

Department of Civil Engineering, University of Colorado, Boulder, CO 80309-0428, U.S.A.

to determine the mixed mode SIFs for cracked discs of anisotropic rock under diametral loading.

In this paper, it is shown that the mixed mode SIFs of anisotropic rocks can be determined by a new formulation of the BEM based on the definition of the J-integral for anisotropic materials and the relative displacements at the crack tip. Numerical examples of determination of the mixed mode SIFs for a Cracked Straight Through Brazilian Disc (CSTBD) specimen are presented for isotropic and anisotropic media. Good agreement is found between the mixed mode SIFs determined by the proposed method and those reported by Atkinson *et al.* [9] for isotropic media. For anisotropic cracked circular discs, the effect of crack length, crack angle, anisotropic orientation and degree of material anisotropy on the values of SIFs is also analyzed.

The most fundamental parameter in fracture mechanics is called the *fracture toughness* indicating the resistance of a material to crack propagation. Fracture toughness is defined as the critical value of the SIF when crack initiation takes place. This implies that the fracture toughness can be obtained by experimental procedures if the SIF is known for a given body under a certain type and magnitude of loading. Earlier measurements of rock fracture toughness [12–16] followed the ASTM-E399 standard method initially suggested for metallic materials. Because most rocks are brittle, fatigue pre-cracking required by that ASTM standard has been found to be very difficult to produce. Testing methods such as the testing of chevron bend specimens and short rod specimens, have been suggested by the ISRM [17]. Both types of specimens have been widely used for determining pure mode I fracture toughness of isotropic rocks by Ingraffea *et al.* [18] on limestone and granite, Swan and Alm [19] and Sun and Ouchterlony [20] on Stripa granite, Senseny and Pfeifle [21] on sandstone and shale, Gunsallus and Kulhawy [22] on sandstone, and Ouchterlony [23] on granite and marble. These two methods have several disadvantages as they require very low failure initiation loads, relatively large amounts of intact rock core, complicated loading fixtures and complex sample preparation for the short rod specimens [10].

These disadvantages can be overcome by conducting a Brazilian test on a Cracked Chevron Notched Brazilian Disc (CCNBD) or a Cracked Straight Through Brazilian Disc (CSTBD) (Fig. 1). The advantages of using the Brazilian test to determine the rock fracture toughness are high failure load, a simple loading fixture and convenient specimen preparation [10]. In addition, it is possible to measure mode I, mode II and mixed mode I–II fracture toughness by inclining the initial crack in the discs at different angles with respect to the diametral load. Shetty *et al.* [24] and Fowell and Xu [10] used the CCNBD geometry to measure the fracture toughness of ceramics and rocks, respectively. This geometry has been suggested by the

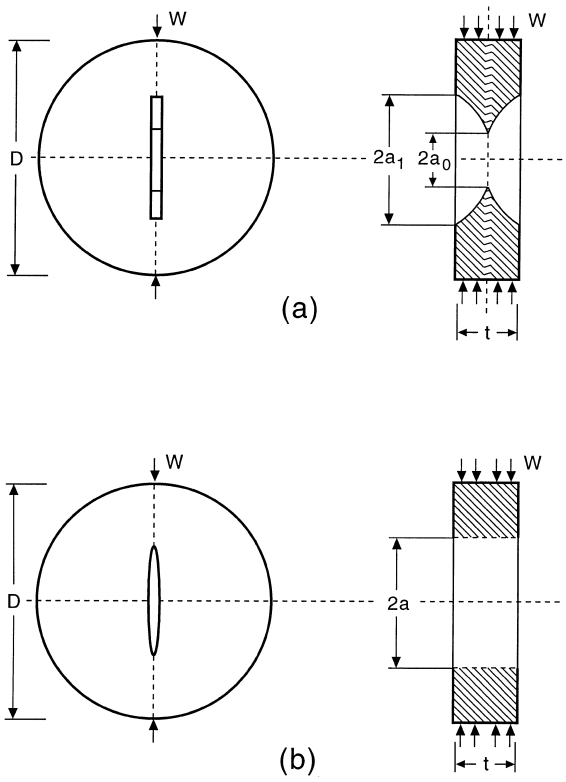

Fig. 1. Cracked Brazilian disc specimens under diametral compression. (a) Cracked Chevron Notched Brazilian Disc (CCNBD), (b) Cracked Straight Through Brazilian Disc (CSTBD).

ISRM [25] for determining mode I fracture toughness of rocks. The CSTBD has also been introduced to determine the mixed mode I–II fracture toughness in isotropic materials by Awaji and Sato [8], Atkinson *et al.* [9], Sanchez [26] and Shetty *et al.* [27]. Hirose *et al.* [28] studied the effect of material anisotropy on the mode I SIF only using the 3D Finite Element Method (FEM).

In this paper, a procedure for determining the fracture toughness of anisotropic rocks under pure mode I and mode II loading is presented. A shale assumed to be transversely isotropic was selected and its fracture toughness was determined by conducting Brazilian tests on CSTBD specimens. It was found that, in general, the fracture toughness of anisotropic rocks depends on the rock properties and the initial crack orientation.

Failure of rock construction frequently takes place following crack growth. Understanding the behavior of crack initiation and propagation is important for evaluating the safety limits of cracked structures. Crack propagation processes are frequently simulated by an incremental crack extension analysis, based on certain failure criterion to predict the direction of crack initiation. For each increment of crack extension, a stress analysis is carried out, and the SIFs are evaluated. Because of the complex geometry, which is continuously changing during crack extension, numerical techniques are required to simulate crack propagation problems. For a long time, the Finite Element

Method (FEM) has been used to determine the SIFs for cracked media. Numerous researchers have employed this method to study fracture propagation processes [29–33]. The main disadvantage of the FEM, when used in the context of modeling crack propagation, is that the finite element mesh has to be updated following each step of crack extension.

Over the past ten years, the boundary element method (BEM) has emerged as an alternative method for the analysis of cracked bodies. However, because the coincidence of the crack surfaces gives rise to a singular system of algebraic equations, the solution of this problem can not be obtained with the direct formulation of the BEM. Some special techniques have been devised to overcome this difficulty such as the sub-regional method [34], the displacement discontinuity method (DDM) [35, 36] and the dual BEM [37–39]. A detailed discussion on these methods can be found in Pan and Amadei [40] where an efficient and accurate BEM formulation was proposed.

Another objective of this paper is the study of crack initiation and propagation in anisotropic rocks subjected to Brazilian loads. A numerical procedure based on the BEM formulation of Pan and Amadei [40] and the maximum tensile stress criterion has been developed to predict the angle of crack initiation and the path of crack propagation in anisotropic rocks. Crack propagation in an anisotropic homogeneous rock disc under mixed mode I–II loading is simulated by an incremental crack extension with a piece-wise linear discretization. A computer program, which can automatically generate a new mesh (required for analyzing sequentially the changing boundary configuration) has been developed to simulate the crack propagation process. Some experimental observations of crack initiation angles and crack propagation were obtained by conducting diametral loading of CSTBD specimens of a shale. It was found that the numerical analysis could predict relatively well the direction of crack initiation and the path of crack propagation. Note that throughout this paper, a generalized plane stress deformation is assumed and tensile stresses and strains are taken as positive.

THEORETICAL BACKGROUND

Anisotropic elasticity

As discussed in Lekhnitskii [41] and in our companion paper [42], the stress and displacement fields in a two-dimensional linear elastic, homogeneous, and anisotropic medium can be formulated in terms of two analytical functions, $\phi_k(z_k)$, of the complex variables $z_k = x + \mu_k y$ ($k = 1, 2$) where, μ_k are the roots of a characteristic equation

$$a_{11}\mu^4 - 2a_{16}\mu^3 + (2a_{12} + a_{66})\mu^2 - 2a_{26}\mu + a_{22} = 0 \quad (1)$$

In Equation (1), a_{11}, a_{12}, ..., a_{66} are the compliance components of the medium in a global coordinate system (x, y) attached to the medium. Lekhnitskii [41] has shown that the roots of this equation are always either complex or purely imaginary, two of them being the conjugate of the two others. Let μ_1, μ_2 be those roots and $\bar{\mu}_1$, $\bar{\mu}_2$ their respective conjugates. Assuming μ_1 and μ_2 to be distinct, the general expressions for the stress and displacement components are [41]

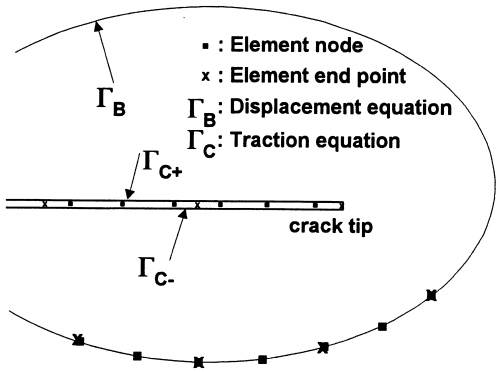

Fig. 2. Geometry of a two-dimensional cracked domain.

$$\begin{aligned}\sigma_x &= 2\mathrm{Re}[\mu_1^2\phi_1'(z_1) + \mu_2^2\phi_2'(z_2)],\\ \sigma_y &= 2\mathrm{Re}[\phi_1'(z_1) + \phi_2'(z_2)],\\ \tau_{xy} &= -2\mathrm{Re}[\mu_1\phi_1'(z_1) + \mu_2\phi_2'(z_2)]\end{aligned} \quad (2)$$

and

$$\begin{aligned}u &= 2\mathrm{Re}[P_{11}\phi_1(z_1) + P_{12}\phi_2(z_2)]\\ v &= 2\mathrm{Re}[P_{21}\phi_1(z_1) + P_{22}\phi_2(z_2)]\end{aligned} \quad (3)$$

where

$$\begin{aligned}P_{1k} &= a_{11}\mu_k^2 + a_{12} - a_{16}\mu_k,\\ P_{2k} &= a_{12}\mu_k + a_{22}/\mu_k - a_{26} \qquad (k = 1, 2).\end{aligned} \quad (4)$$

Boundary integral equation

The traditional displacement boundary integral equation for linear elasticity can be expressed as [40]

$$c_{ij}(z_k^0)u_j(z_k^0) + \int_\Gamma T_{ij}(z_k, z_k^0)u_j(z_k)\,\mathrm{d}\Gamma(z_k) = \int_\Gamma U_{ij}(z_k, z_k^0)t_j(z_k)\,\mathrm{d}\Gamma(z_k) \quad (5)$$

where $i, j, k = 1, 2$; T_{ij} and U_{ij} are the Green's tractions and displacements given in Appendix A; c_{ij} are quantities that depend on the geometry of the boundary and are equal to $\delta_{ij}/2$ for a smooth boundary; and z_k and z_k^0 are the field and source points on the boundary Γ of the domain. Discretization of Equation (5) gives a linear system of algebraic equations which can be solved for the unknowns on the boundary. However, for a cracked elastic medium, Equation (5) is not sufficient for solving all the unknowns along the outer boundary of the problem as well as along the two sides of the crack surfaces because of the geometric singularity associated with the crack surface.

In the BEM formulation of Pan and Amadei [40] for cracked anisotropic media, the displacement integral equation is collocated on the outer boundary only and the traction integral equation on one side of the crack only. The displacement integral equation applied to the outer boundary results in the following form ($z^0_{k,\mathrm{B}} \in \Gamma_B$ only, Fig. 2)

$$\begin{aligned} c_{ij}(z^0_{k,\mathrm{B}})u_j(z^0_{k,\mathrm{B}}) + \int_{\Gamma_\mathrm{B}} T_{ij}(z_{k,\mathrm{B}}, z^0_{k,\mathrm{B}})u_j(z_{k,\mathrm{B}})\,\mathrm{d}\Gamma(z_{k,\mathrm{B}}) \\ + \int_{\Gamma_\mathrm{C}} T_{ij}(z_{k,\mathrm{C}}, z^0_{k,\mathrm{B}})[u_j(z_{k,\mathrm{C}+}) \\ - u_j(z_{k,\mathrm{C}-})]\,\mathrm{d}\Gamma(z_{k,\mathrm{C}}) \\ = \int_{\Gamma_\mathrm{B}} U_{ij}(z_{k,\mathrm{B}}, z^0_{k,\mathrm{B}})t_j(z_{k,\mathrm{B}})\,\mathrm{d}\Gamma(z_{k,\mathrm{B}}) \quad (6) \end{aligned}$$

where Γ_C has the same outward normal as $\Gamma_{\mathrm{C}+}$. Here, the subscripts B and C denote the outer boundary and the crack surface, respectively.

The traction integral equation (for z^0_k being a smooth point on the crack) applied to one side of the crack surfaces is ($z^0_{k,\mathrm{C}} \in \Gamma_{C+}$ only)

$$\begin{aligned} 0.5t_l(z^0_{k,\mathrm{C}}) + n_m(z^0_{k,\mathrm{C}}) \int_{\Gamma_\mathrm{B}} c_{lmik} T_{ij,k}(z^0_{k,\mathrm{C}}, z_{k,\mathrm{B}})u_j(z_{k,\mathrm{B}})\,\mathrm{d}\Gamma(z_{k,\mathrm{B}}) \\ + n_m(z^0_{k,\mathrm{C}}) \int_{\Gamma_\mathrm{C}} c_{lmik} T_{ij,k}(z^0_{k,\mathrm{C}}, z_{k,\mathrm{C}})[u_j(z_{k,\mathrm{C}+}) \\ - u_j(z_{k,\mathrm{C}-})]\,\mathrm{d}\Gamma(z_{k,\mathrm{C}}) = n_m(z^0_{k,\mathrm{C}}) \int_{\Gamma_\mathrm{B}} c_{lmik} U_{ij,k} \\ \times (z^0_{k,\mathrm{C}}, z_{k,\mathrm{B}})t_j(z_{k,\mathrm{B}})\,\mathrm{d}\Gamma(z_{k,\mathrm{B}}) \quad (7) \end{aligned}$$

where n_m is the unit outward normal to the contour path; and the gradient tensors $T_{ij,k}$ and $U_{ij,k}$ denote differentiation with respect to the source coordinate x^0_k or y^0_k.

The Cauchy singularity in the displacement Equation (6) can be avoided by the rigid-body motion method. The integrand on the right-hand side of Equation (6) has only integrable singularity which can be resolved by the bi-cubic transformation method [44]. The hyper-singularity in the traction integral Equation (7) is resolved by a new Gauss quadrature formula [40] which is very similar to the traditional weighted Gauss quadrature but with a different weight. Therefore, Equations (6) and (7) can be solved simultaneously for the unknown displacements or tractions on the outer boundary and the unknown crack displacement differences on the crack surface.

Calculation of stress intensity factors

The mixed mode stress intensity factors for anisotropic media can be determined by using the J-integral combined with a decoupling technique [40, 45]. This technique is based on the ratio of relative crack tip displacements calculated with the BEM. The contour-independent J-integral is defined as [46]

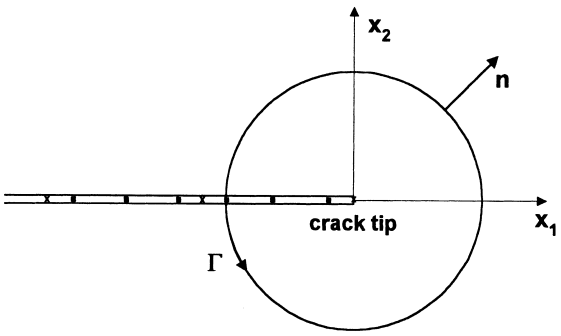

Fig. 3. Contour path of J-integral.

$$J_k = \sum_{i,j=1}^{2} \int_\Gamma \left(\frac{1}{2}\sigma_{ij}\varepsilon_{ij}n_k - \sigma_{ji}n_i u_{j,k} \right) \mathrm{d}\Gamma \quad (8)$$

where $k = 1, 2$; Γ is a generic contour surrounding the crack tip (Fig. 3); σ_{ij} and ε_{ij} are the stress and strain tensors, respectively; and n_i are the components of the unit outward normal to the contour path.

Chu and Hong [47] have shown that for a cracked two-dimensional homogeneous and anisotropic body, the J_1 and J_2 integrals are related to the stress intensity factors K_I and K_{II} by the following relations

$$\begin{aligned} J_1 &= \alpha_{11}K_\mathrm{I}^2 + \alpha_{12}K_\mathrm{I}K_\mathrm{II} + \alpha_{22}K_\mathrm{II}^2, \\ J_2 &= \beta_{11}K_\mathrm{I}^2 + \beta_{12}K_\mathrm{I}K_\mathrm{II} + \beta_{22}K_\mathrm{II}^2 \end{aligned} \quad (9)$$

where α_{ij} and β_{ij} are constants related to the elastic properties of the anisotropic medium. The detailed relations between α_{ij}, β_{ij} and the elastic constants can be found in Chu and Hong [47]. By expanding the displacements near the crack tip, the ratio of relative displacements is found to be [40, 45]

$$\lambda \equiv \frac{u_2^+ - u_2^-}{u_1^+ - u_1^-} = \frac{H_{21}K_\mathrm{I} + H_{22}K_\mathrm{II}}{H_{11}K_\mathrm{I} + H_{12}K_\mathrm{II}} \quad (10)$$

where λ is the ratio of the relative crack-tip displacements obtained by the extrapolation method [40], and

$$\begin{aligned} H_{11} &= \mathrm{Im}\left(\frac{\mu_2 P_{11} - \mu_1 P_{12}}{\mu_1 - \mu_2} \right); \\ H_{12} &= \mathrm{Im}\left(\frac{P_{11} - P_{12}}{\mu_1 - \mu_2} \right); \\ H_{21} &= \mathrm{Im}\left(\frac{\mu_2 P_{21} - \mu_1 P_{22}}{\mu_1 - \mu_2} \right); \\ H_{22} &= \mathrm{Im}\left(\frac{P_{21} - P_{22}}{\mu_1 - \mu_2} \right). \end{aligned} \quad (11)$$

From Equation (10), the ratio of stress intensity factors is equal to

$$\rho = \frac{K_\mathrm{I}}{K_\mathrm{II}} = \frac{\lambda H_{12} - H_{22}}{H_{21} - \lambda H_{11}}. \quad (12)$$

Substituting Equation (12) into Equation (9), the mode II SIF, K_{II}, can be expressed as follows

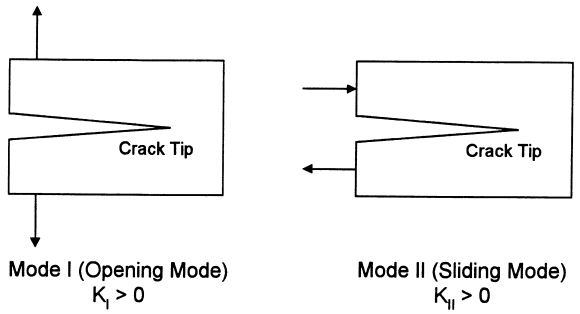

Fig. 4. Sign convention used for determining SIFs in mode I and mode II.

$$K_{\mathrm{II}} = \sqrt{\frac{J_1}{\alpha_{11}\rho^2 + \alpha_{12}\rho + \alpha_{22}}}. \tag{13}$$

Once K_{II} is calculated from Equation (13), $K_{\mathrm{I}} = \rho K_{\mathrm{II}}$. In this paper, the sign convention for the corresponding SIFs (K_{I} and K_{II}) is shown in Fig. 4. Using the relative crack-tip displacements, the sign of the SIFs can then be determined.

Direction of crack initiation

In fracture mechanics, there are three criteria commonly used to predict the crack initiation angle: the maximum tensile stress criterion, or σ-criterion [48]; the maximum energy release rate criterion, or G-criterion [49]; and the minimum strain energy density criterion, or S-criterion [50]. Among them, the σ-criterion has been found to predict well the directions of crack initiation compared to the experimental results for polymethylmethacrylate [51, 52] and brittle clay [53]. Because of its simplicity, the σ-criterion seems to be the most popular criterion in mixed mode I–II fracture studies [54]. Therefore, the σ-criterion was used in this study to determine the crack initiation angle for anisotropic rocks. It is noteworthy that in order to compute the loads required to propagate a crack, other criteria need to be used [49, 50].

For anisotropic materials, the general form of the elastic stress field near the crack tip in the local Cartesian coordinates x'', y'' of Fig. 5 can be expressed in terms of the two stress intensity factors K_{I} and K_{II} as follows [43]

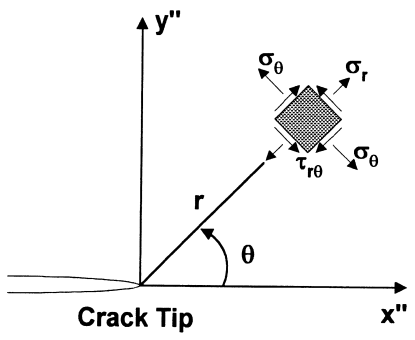

Fig. 5. Crack tip coordinate system and stress components.

$$\begin{aligned}
\sigma_{x''} &= \frac{K_{\mathrm{I}}}{\sqrt{2\pi r}}\mathrm{Re}\left[\frac{\mu_1\mu_2}{\mu_1-\mu_2}\left(\frac{\mu_2}{\sqrt{\cos\theta+\mu_2\sin\theta}}\right.\right.\\
&\quad\left.\left.-\frac{\mu_1}{\sqrt{\cos\theta+\mu_1\sin\theta}}\right)\right]+\frac{K_{\mathrm{II}}}{\sqrt{2\pi r}}\\
&\quad\times\mathrm{Re}\left[\frac{1}{\mu_1-\mu_2}\left(\frac{\mu_2^2}{\sqrt{\cos\theta+\mu_2\sin\theta}}\right.\right.\\
&\quad\left.\left.-\frac{\mu_1^2}{\sqrt{\cos\theta+\mu_1\sin\theta}}\right)\right],\\
\sigma_{y''} &= \frac{K_{\mathrm{I}}}{\sqrt{2\pi r}}\mathrm{Re}\left[\frac{1}{\mu_1-\mu_2}\left(\frac{\mu_1}{\sqrt{\cos\theta+\mu_2\sin\theta}}\right.\right.\\
&\quad\left.\left.-\frac{\mu_2}{\sqrt{\cos\theta+\mu_1\sin\theta}}\right)\right]+\frac{K_{\mathrm{II}}}{\sqrt{2\pi r}}\mathrm{Re}\left[\frac{1}{\mu_1-\mu_2}\right.\\
&\quad\left.\times\left(\frac{1}{\sqrt{\cos\theta+\mu_2\sin\theta}}-\frac{1}{\sqrt{\cos\theta+\mu_1\sin\theta}}\right)\right],\\
\tau_{x''y''} &= \frac{K_{\mathrm{I}}}{\sqrt{2\pi r}}\mathrm{Re}\left[\frac{\mu_1\mu_2}{\mu_1-\mu_2}\left(\frac{1}{\sqrt{\cos\theta+\mu_1\sin\theta}}\right.\right.\\
&\quad\left.\left.-\frac{1}{\sqrt{\cos\theta+\mu_2\sin\theta}}\right)\right]+\frac{K_{\mathrm{II}}}{\sqrt{2\pi r}}\mathrm{Re}\left[\frac{1}{\mu_1-\mu_2}\right.\\
&\quad\left.\times\left(\frac{\mu_1}{\sqrt{\cos\theta+\mu_1\sin\theta}}-\frac{\mu_2}{\sqrt{\cos\theta+\mu_2\sin\theta}}\right)\right]
\end{aligned} \tag{14}$$

where μ_1 and μ_2 are the roots of the characteristic equation (Equation (1)).

Using coordinate transformation, the stress field near the crack tip in the polar coordinates (r, θ) of Fig. 5 is such that

$$\begin{aligned}
\sigma_\theta &= \frac{\sigma_{x''}+\sigma_{y''}}{2}-\frac{\sigma_{x''}-\sigma_{y''}}{2}\cos 2\theta-\tau_{x''y''}\sin 2\theta,\\
\tau_{r\theta} &= -\frac{\sigma_{x''}-\sigma_{y''}}{2}\sin 2\theta+\tau_{x''y''}\cos 2\theta.
\end{aligned} \tag{15}$$

If the maximum σ-criterion is used, the angle of crack initiation, θ_0, must satisfy

$$\frac{\partial\sigma_\theta}{\partial\theta}=0\ (\text{or } \tau_{r\theta}=0)\quad\text{and}\quad\frac{\partial^2\sigma_\theta}{\partial\theta^2}<0. \tag{16}$$

A numerical procedure was applied to find the angle θ_0 when σ_θ is a maximum for known values of the material elastic constants, the anisotropic orientation angle ψ and the crack geometry.

Crack propagation process

In this study, the process of crack propagation in an anisotropic homogeneous rock disc under mixed mode I–II loading is simulated by incremental crack extension with a piece-wise linear discretization. For each incremental analysis, crack extension is conveniently modeled by a new boundary element. A computer program has been developed to automatically generate

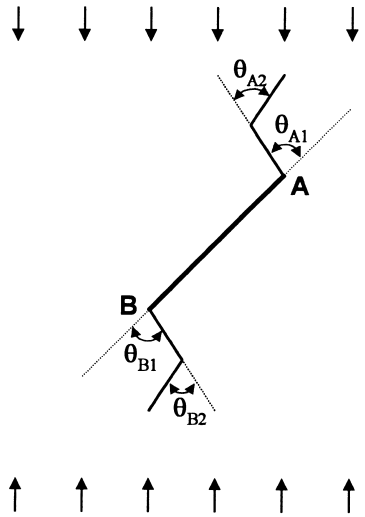

Fig. 6. Process of crack propagation by increasing the number of linear elements.

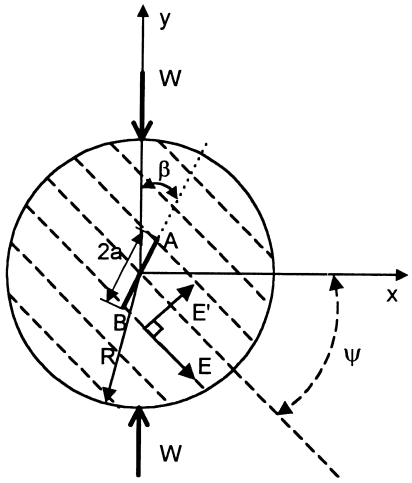

Fig. 7. Geometry of a Cracked Straight Through Brazilian Disc (CSTBD) specimen of anisotropic rock under diametral loading.

Table 1. Normalized stress intensity factors for a central slant crack in an isotropic Brazilian disc subjected to a concentrated load ($a/R = 0.5$)

	Atkinson *et al.* [9]		This study	
β (Rad.)	K_I/K_0	K_{II}/K_0	K_I/K_0	K_{II}/K_0
0	1.387	0	1.339	0
$\pi/16$	0.970	−1.340	0.960	−1.275
$2\pi/16$	0.030	−2.113	0.074	−2.061
$3\pi/16$	−0.946	−2.300	−0.903	−2.275
$\pi/4$	−1.784	−2.132	−1.737	−2.103
$5\pi/16$	−2.446	−1.728	−2.377	−1.711
$6\pi/16$	−2.885	−1.188	−2.826	−1.197
$7\pi/16$	−3.127	−0.604	−3.092	−0.614
$\pi/2$	−3.208	0	−3.180	0

Table 2. Normalized stress intensity factors for a central slant crack in an isotropic Brazilian disc subjected to a concentrated load ($\beta = 45^\circ$)

	Atkinson *et al.* [9]		This study	
a/R	K_I/K_0	K_{II}/K_0	K_I/K_0	K_{II}/K_0
0.1	−1.035	−2.010	−1.020	−1.968
0.2	−1.139	−2.035	−1.116	−1.995
0.3	−1.306	−2.069	−1.272	−2.036
0.4	−1.528	−2.100	−1.484	−2.069
0.5	−1.784	−2.132	−1.737	−2.103
0.6	−2.048	−2.200	−2.020	−2.148
0.7	–	–	−2.337	−2.213

Table 3. Three sets of dimensionless elastic constants ($v = 0.25$)

	E/E'					E/G'					v'				
Case I	1/3	1/2	1	2	3			2.5					0.25		
Case II			1			0.5	1.5	2.5	3.5	4.5			0.25		
Case III			1					2.5			0.05	0.15	0.25	0.35	0.45

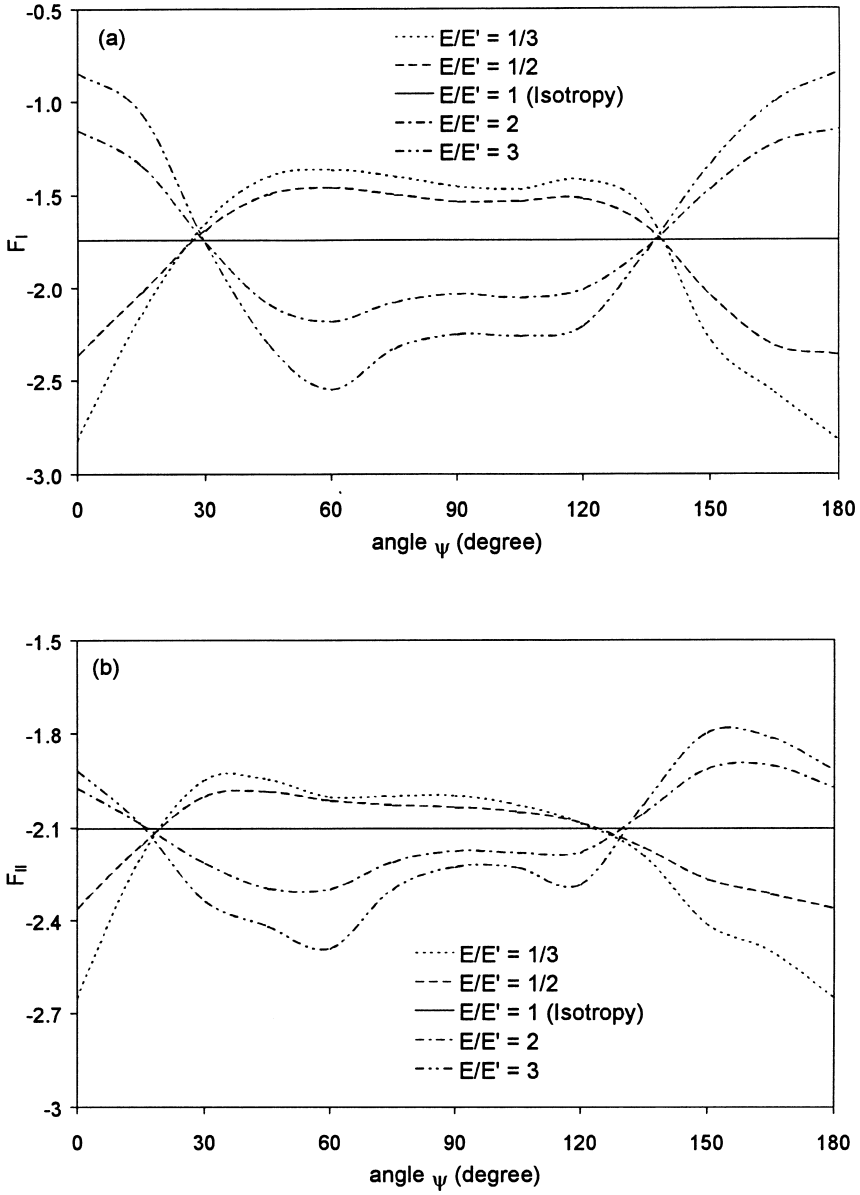

Fig. 8. Variation of F_{I} in (a) and F_{II} in (b) with the material orientation angle ψ for case I ($a/R = 0.5$, $\beta = 45°$, $E/G' = 2.5$, $\nu' = 0.25$).

new data required for analyzing sequentially the changing boundary configuration. Based on the calculation of the SIFs and crack initiation angle for each increment, the procedure of crack propagation can be simulated. The steps in the crack propagation process are summarized as follows (Fig. 6):

(1) Compute the SIFs using the proposed BEM;

(2) Determine the angle of crack initiation based on the maximum tensile stress criterion;

(3) Extend the crack by a linear element (of length selected by the user) along the direction determined in step 2;

(4) Automatically generate the new BEM mesh;

(5) Repeat all the above steps until the new crack is near the outer boundary.

NUMERICAL EXAMPLES OF STRESS INTENSITY FACTORS

The geometry of the problem analyzed here is that of a thin circular disc of radius R and thickness t with a central crack of length $2a$, loaded by a pair of concentrated and diametral compressive loads W (Fig. 7). The outer boundary and the crack surface are discretized with 28 continuous and 10 discontinuous quadratic elements, respectively. The sign convention of the corresponding SIFs in mode I and mode II is shown in Fig. 4. The normalized SIFs, defined as F_{I} and F_{II}, are equal to

$$F_{\mathrm{I}} = \frac{K_{\mathrm{I}}}{K_0}; \qquad F_{\mathrm{II}} = \frac{K_{\mathrm{II}}}{K_0} \tag{17}$$

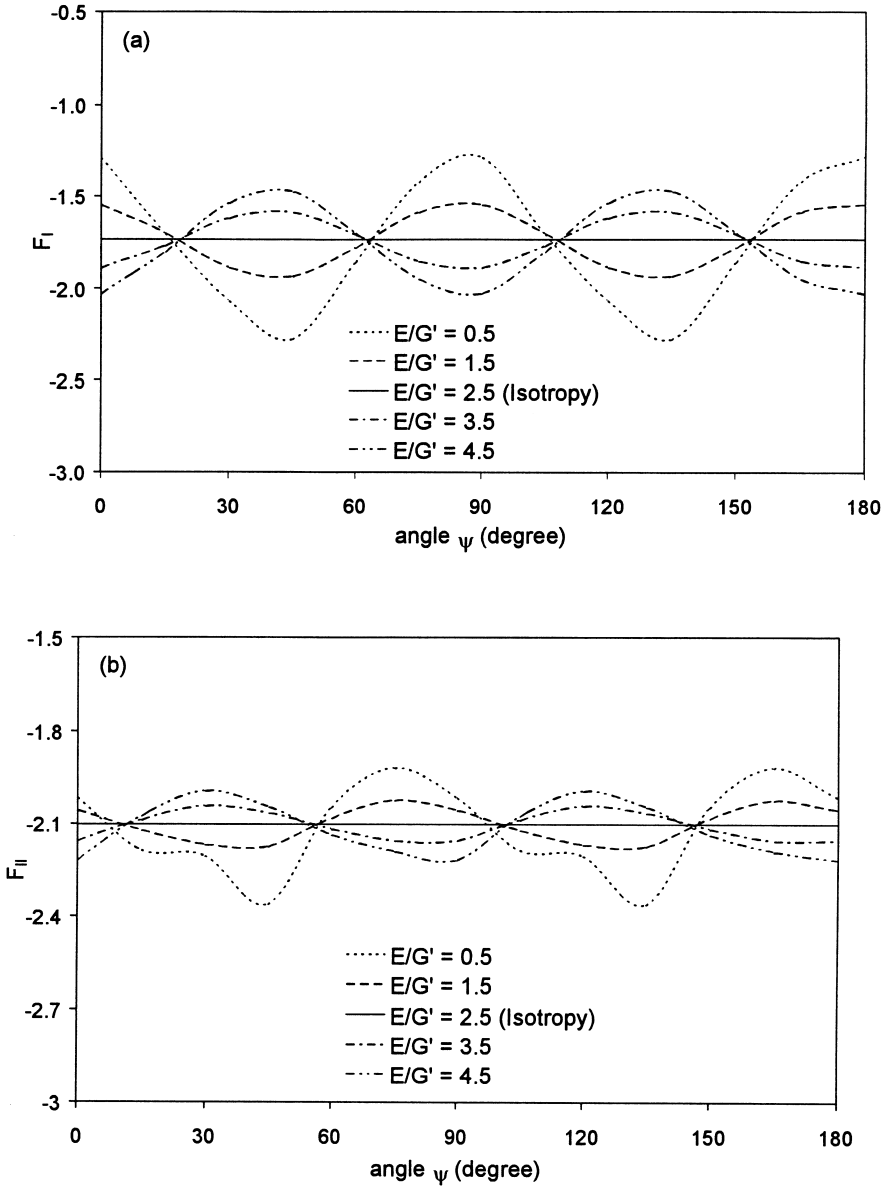

Fig. 9. Variation of F_I in (a) and F_{II} in (b) with the material orientation angle ψ for case II ($a/R = 0.5$, $\beta = 45^\circ$, $E/E' = 1$, $\nu' = 0.25$).

with

$$K_0 = \frac{W}{\pi R t}\sqrt{\pi a}. \tag{18}$$

Example 1 — Isotropic case

In order to compare our results with existing published results, an isotropic and cracked Brazilian disc with a central slant crack is considered. Two cases are analyzed: (1) $a/R = 0.5$, the crack angle β varies between 0 and $\pi/2$, and (2) $\beta = 45^\circ$, a/R varies between 0.1 and 0.7. The two normalized SIFs, F_I and F_{II}, calculated with the BEM program for these two cases are compared with those obtained numerically by Atkinson *et al.* [9] using the continuously distributed dislocation method. The results are shown in Tables 1 and 2. In general, good agreement is found between the two methods.

Example 2 — Anisotropic case

In order to evaluate the influence of material anisotropy on the SIFs, consider again the disc of Fig. 7. The disc consists of an anisotropic material with a central slant crack inclined with respect to a pair of concentrated diametral compressive loads. The crack angle β is fixed at 45° and the crack length is such that $a/R = 0.5$. The material is transversely isotropic with the plane of transverse isotropy inclined at an angle ψ with respect to the x-axis. The material has five independent elastic constants (E, E', ν, ν', and G') in the local coordinate system: E and E' are the Young's moduli in the plane of transverse isotropy and in a direction normal to it, respectively; ν and ν' are the Poisson's ratios characterizing the lateral strain response in the plane of transverse isotropy to a stress acting parallel and normal to it, respectively; and G' is the shear modulus in the planes normal to the plane of

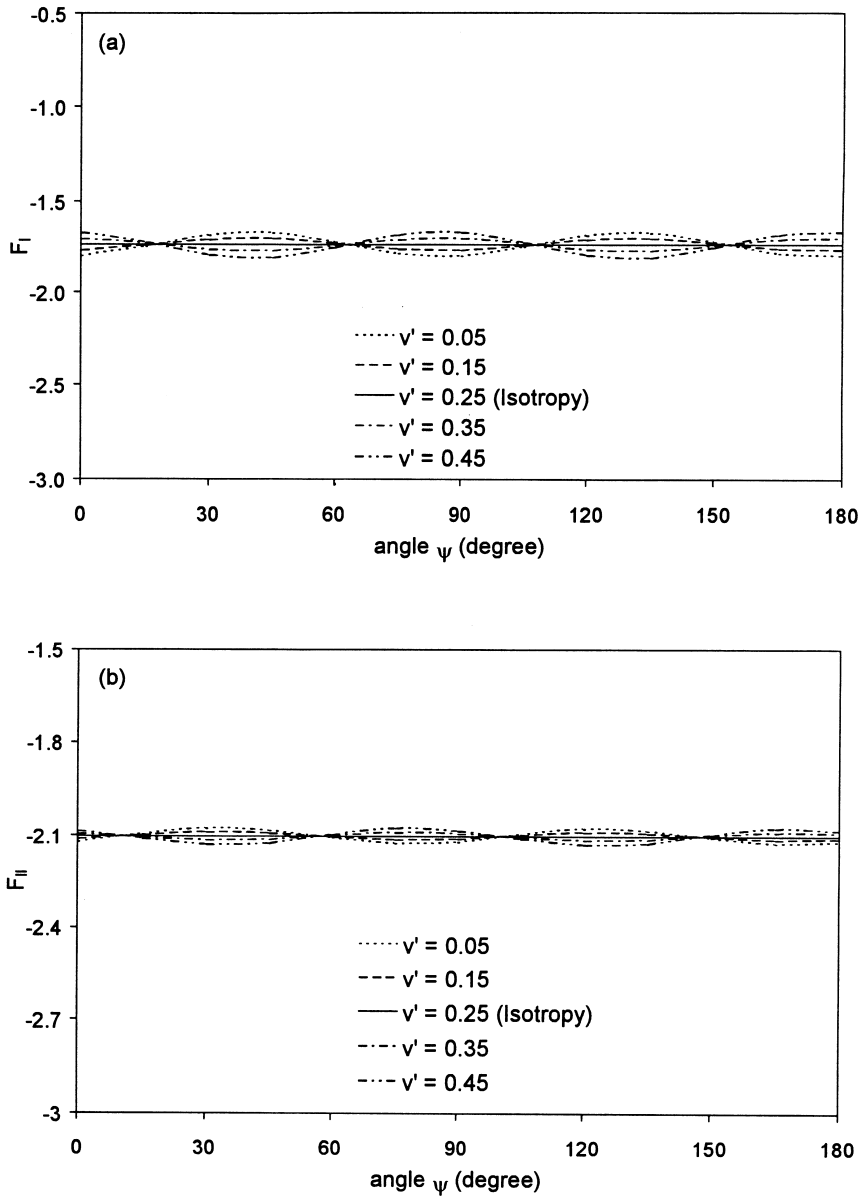

Fig. 10. Variation of F_I in (a) and F_{II} in (b) with the material orientation angle ψ for case III ($a/R = 0.5$, $\beta = 45°$, $E/E' = 1$, $E/G' = 2.5$).

transverse isotropy. In this example, the angle ψ varies from 0° to 180°. Three sets of dimensionless elastic constants are considered and are defined as cases I, II and III in Table 3. The numerical results are plotted in Figs 8–10 for cases I, II and III, respectively. The results for the isotropic case ($E/E' = 1$, $E/G' = 2.5$, and $\nu' = 0.25$) are also shown for comparison as solid lines in Figs 8–10. Analysis of Figs 8–10 reveals several major trends:

(1) For cases I and II, the orientation of the planes of rock anisotropy with respect to the horizontal plane has a strong influence on the value of the SIFs. The influence is small for case III. This means that the effect of E/E' and E/G' on the SIFs is more important than that of ν'.

(2) When $E/E' = 1$ (Figs 9 and 10, cases II and III, respectively), the variation of the SIFs with the angle ψ is periodic with a 90° period. However, this periodicity is not observed for case I (Fig. 8).

(3) There is a greater variation in the SIFs with the orientation angle ψ for materials having a high degree of anisotropy ($E/E' = 3$ or $1/3$; $E/G' = 0.5$ or 4.5).

(4) Fig. 8 indicates that the maximum absolute values of the SIFs occur when the material orientation is about 60° for $E/E' > 1$, and when the loading is perpendicular to the plane of transverse isotropy (i.e. $\psi = 0°$ or 180°) for $E/E' < 1$.

Example 3 — Effect of crack angle β when $\psi = 0°$

The variation of the SIFs with the crack angle β for cases I, II and III is considered in this example by taking $a/R = 0.5$, $\psi = 0°$, and β to vary from 0° to 90°. The variations of the SIFs with the crack angle β are shown in Fig. 11–13 for cases I, II and III, respectively.

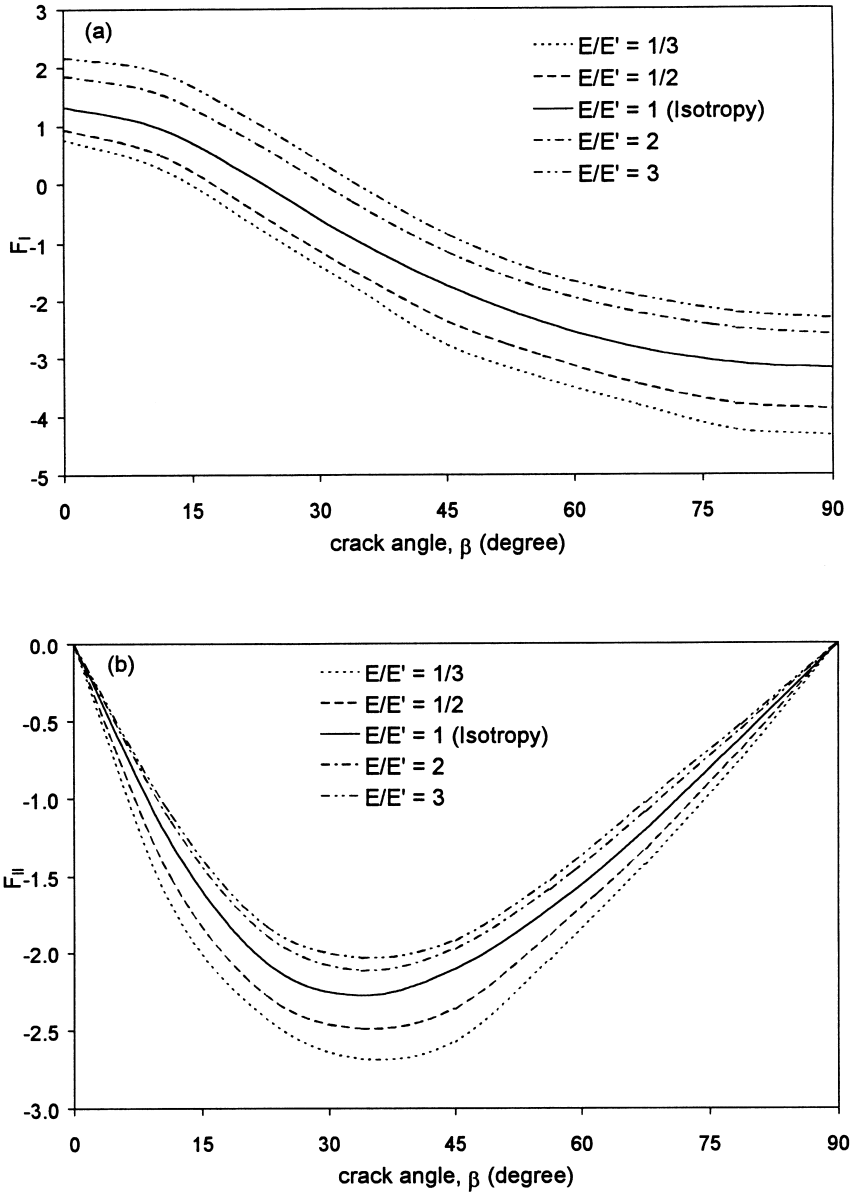

Fig. 11. Variation of F_{I} in (a) and F_{II} in (b) with the crack angle β for case I ($a/R = 0.5$, $\psi = 0°$, $E/G' = 2.5$, $\nu' = 0.25$).

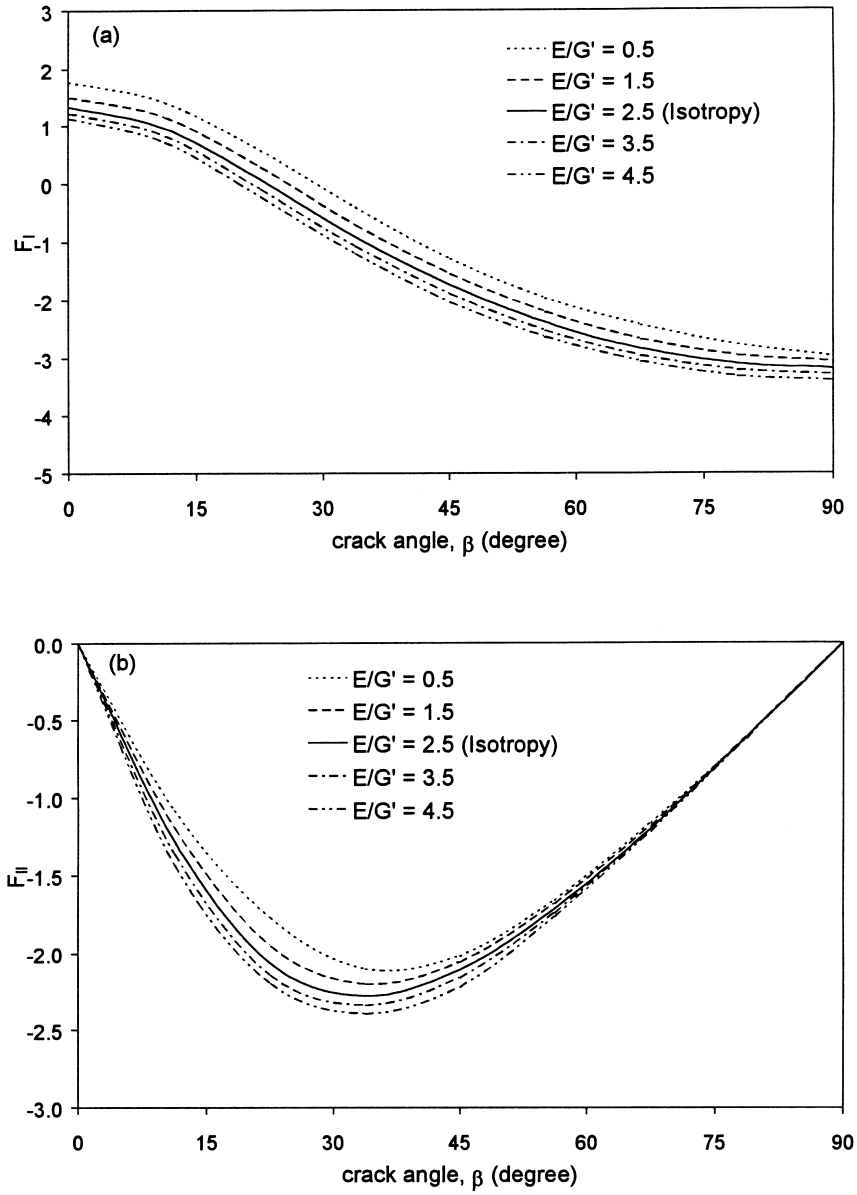

Fig. 12. Variation of F_{I} in (a) and F_{II} in (b) with the crack angle β for case II ($a/R = 0.5$, $\psi = 0^{\circ}$, $E/E' = 1$, $\nu' = 0.25$).

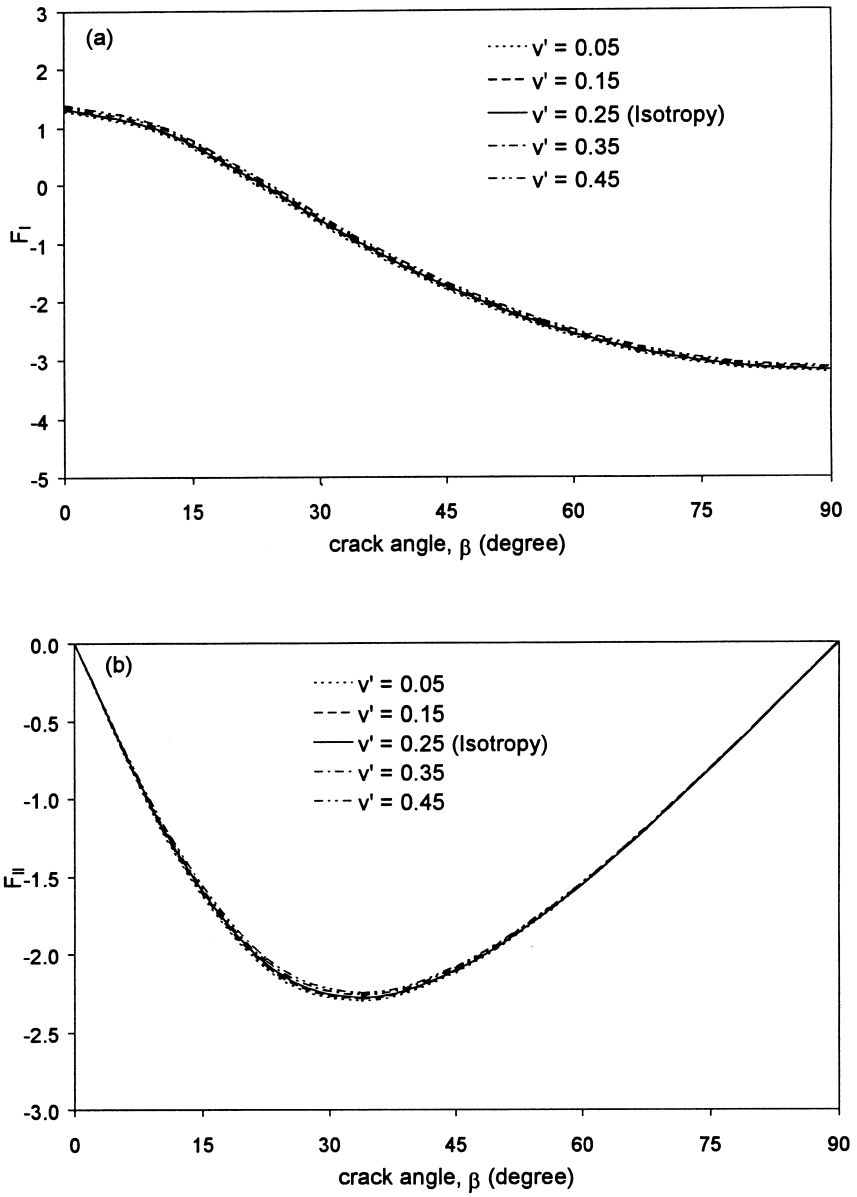

Fig. 13. Variation of F_I in (a) and F_{II} in (b) with the crack angle β for case III ($a/R = 0.5$, $\psi = 0°$, $E/E' = 1$, $E/G' = 2.5$).

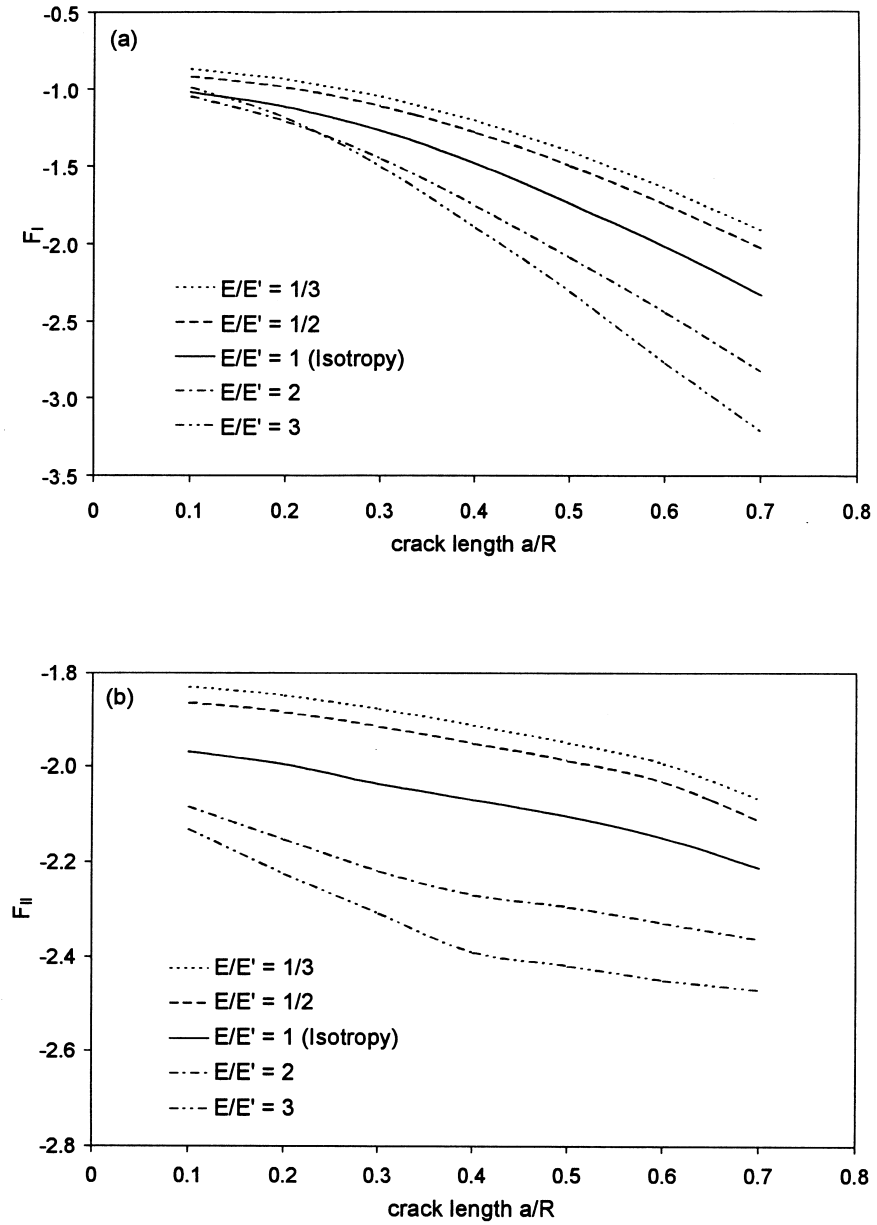

Fig. 14. Variation of F_{I} in (a) and F_{II} in (b) with the crack length a/R for case I ($\beta = \psi = 45^{\circ}$, $E/G' = 2.5$, $\nu' = 0.25$).

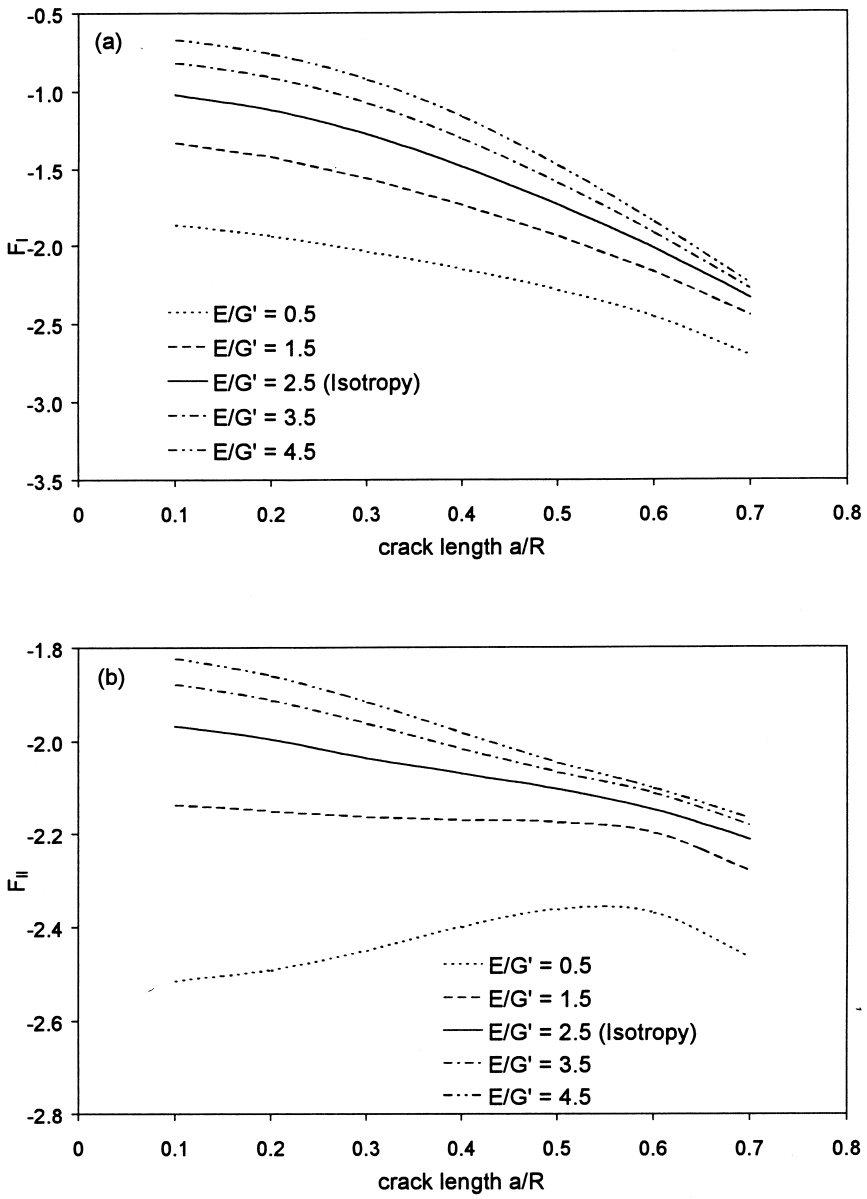

Fig. 15. Variation of F_I in (a) and F_{II} in (b) with the crack length a/R for case II ($\beta = \psi = 45°$, $E/E' = 1$, $\nu' = 0.25$).

For all cases, the mode I SIF reaches a positive maximum value when the crack is parallel to the applied load (i.e., $\beta = 0°$) and decreases smoothly to a negative minimum when the crack is perpendicular to the load (i.e., $\beta = 90°$). The mode II SIF vanishes when the crack angle $\beta = 0°$ or $90°$ and reaches a maximum absolute value when the crack is oriented at about $\beta = 30°$. It can be noted that E/E' has the greatest effect on the SIFs, that E/G' has the next greatest, and that the influence of ν' is almost negligible. For a fixed crack angle β, an increase in E/E' is accompanied with an increase in the values of F_I and F_{II} (Fig. 11).

Example 4 — Effect of crack length a/R when $\beta = \psi = 45°$

The influence of the crack length on the mixed mode SIFs is considered in this example. The disc is such that $\beta = \psi = 45°$. The crack length a/R varies from 0.1 to 0.7, and the material constants are again taken from Table 3. The results are plotted in Figs 14–16.

A wide variation of the SIFs with the crack length is found for cases I and II, whereas the change is small for case III. For case I, F_I approaches its value for an isotropic medium (solid line) when the crack length decreases [Fig. 14(a)]. The opposite trend is found for cases II and III [Fig. 15(a) and Fig. 16(a)]. It can also be noted that longer crack lengths are associated, in general, with higher absolute values of the SIFs.

DETERMINATION OF FRACTURE TOUGHNESS

The mixed mode SIFs for cracked discs of anisotropic rocks under Brazilian loading can be accurately determined with the proposed BEM formulation. Hence, the rock fracture toughness can be easily computed by conducting Brazilian tests on cracked discs. This method was applied to CSTBD specimens of a

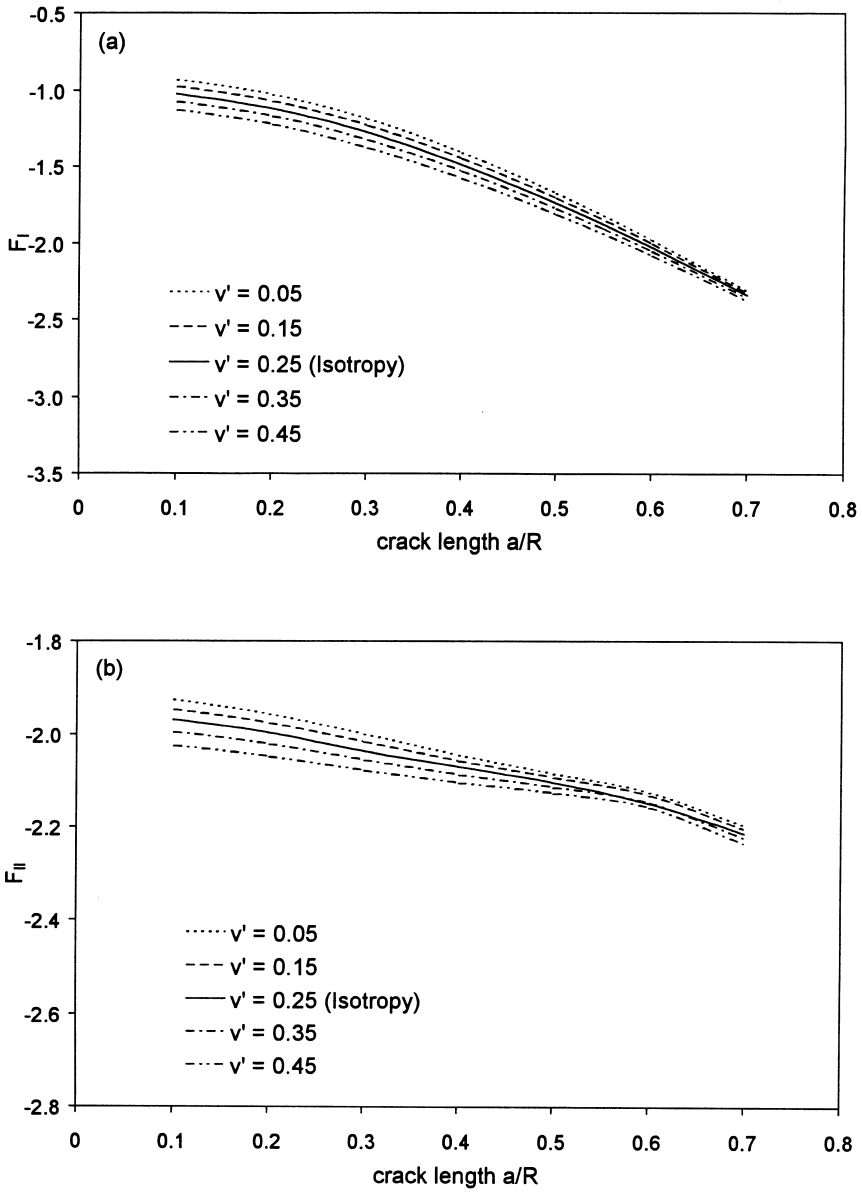

Fig. 16. Variation of F_I in (a) and F_{II} in (b) with the crack length a/R for case III ($\beta = \psi = 45^\circ$, $E/E' = 1$, $E/G' = 2.5$).

Table 4. CSTBD specimen characteristics

	Sample	β (deg.)	D (in.)	t (in.)	$2a$ (in.)	a/R
$\psi = 0^\circ$	SA1-1	0	2.76	0.327	0.795	0.288
	SA1-2	0	2.76	0.350	0.827	0.300
	SA2-1	28.2	2.76	0.374	0.772	0.280
	SA2-2	28.2	2.76	0.343	0.795	0.288
$\psi = 45^\circ$	SB1-1	0.8	2.76	0.354	0.787	0.285
	SB1-2	0.8	2.76	0.327	0.780	0.283
	SB2-1	27.6	2.76	0.366	0.764	0.277
	SB2-2	27.6	2.76	0.374	0.756	0.274
$\psi = 90^\circ$	SC1-1	0	2.76	0.417	0.821	0.297
	SC1-2	0	2.76	0.402	0.848	0.307
	SC2-1	25.9	2.76	0.371	0.795	0.288
	SC2-2	25.9	2.76	0.366	0.807	0.292

(1 in = 25.4 mm).

Table 5. Elastic constants of the shale

	E ($\times 10^6$ psi)	E' ($\times 10^6$ psi)	ν	ν'	G' ($\times 10^6$ psi)
Shale	2.95	2.41	0.462	0.339	0.97

(10^6 psi = 6.89 GPa).

shale assumed to be transversely isotropic with the plane of transverse isotropy parallel to the apparent shale layers. The geometry of the testing specimens is shown in Fig. 7.

Determination of the fracture toughness of the shale first requires determination of its elastic constants. This was done using the results of Brazilian tests on uncracked discs. Details of the methodology to determine the elastic constants using Brazilian tests can be found in the companion paper [42].

Experimental procedure

Core samples with a diameter $D = 2.76$ in. were (70.10 mm) obtained from a block of shale by drilling in a direction parallel to apparent planes of rock anisotropy. Disc specimens with a thickness-to-diameter ratio t/D of about 0.13 were prepared. Their end faces were flat to within 0.01 in. (0.25 mm) and parallel to within 0.25°. A circular diamond saw with a diameter of 0.88 in. (22.35 mm) and a thickness of 0.01 in. (0.25 mm) was used to cut the required chevron notch. The notch was made with two cuts on both sides of

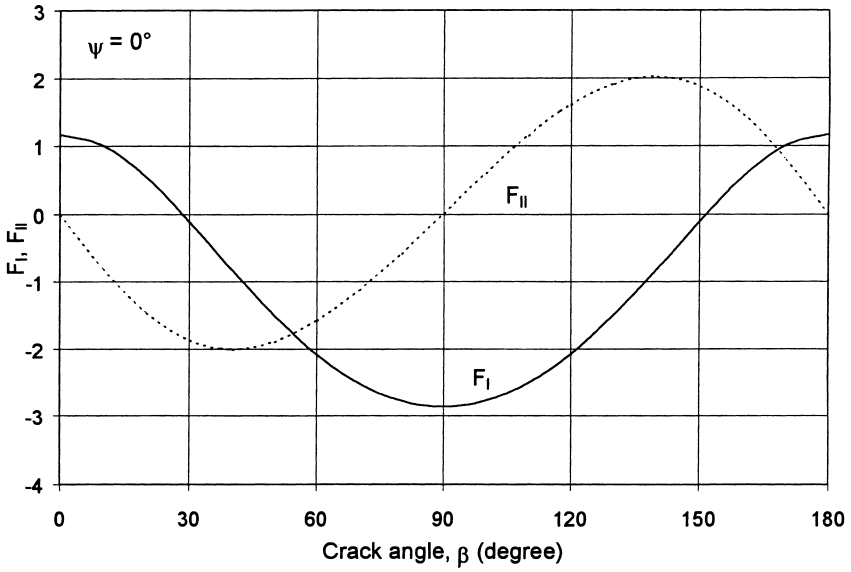

Fig. 17. Variation of normalized SIFs with the crack angle β for $\psi = 0°$.

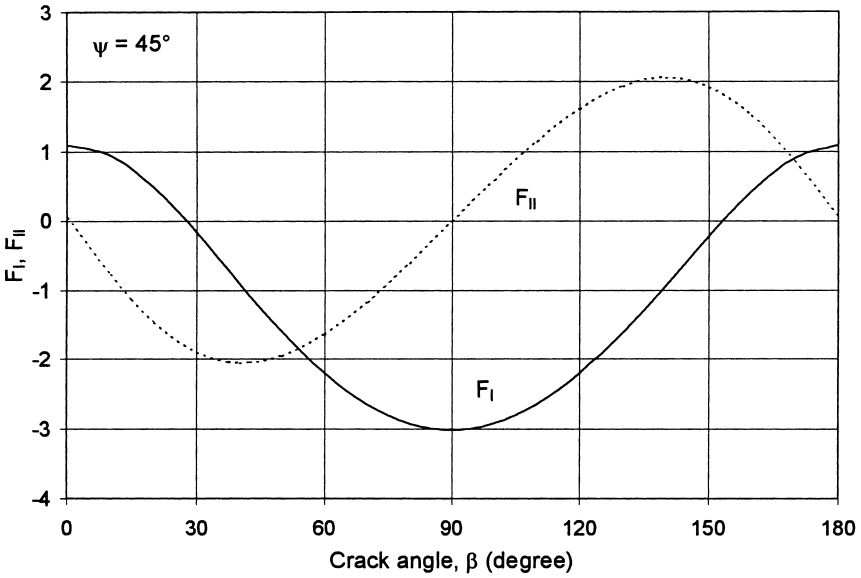

Fig. 18. Variation of normalized SIFs with the crack angle β for $\psi = 45°$.

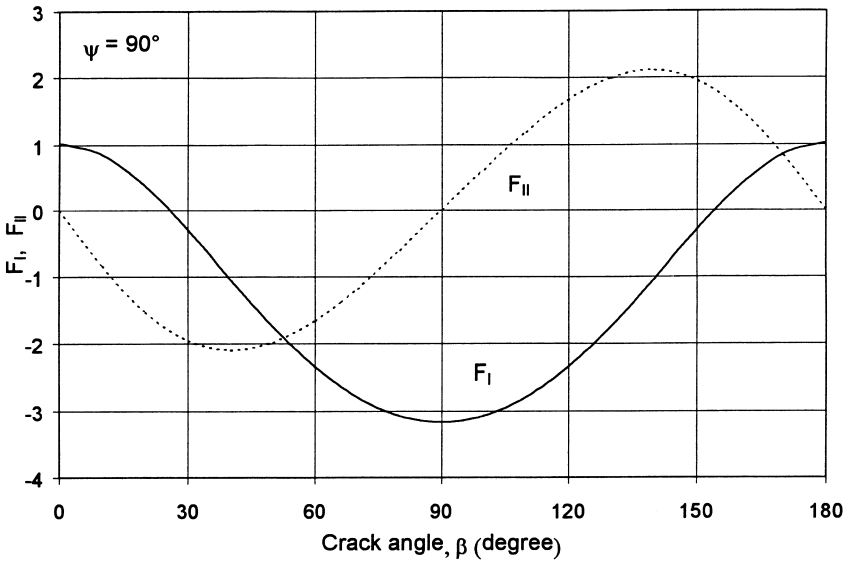

Fig. 19. Variation of normalized SIFs with the crack angle β for $\psi = 90°$.

the disc along the designed crack orientation direction on the same diametral cutting plane. A check was made to ensure that the cutting was done exactly at the center of the disc surface and in a direction perpendicular to the disc surfaces. Then, using a tiny line saw with a thickness of 0.017 in. (0.43 mm) to cut down the V-shaped convex parts, the CSTBD specimens were made. After preparation, the CSTBD specimens had a crack with a thickness less than 0.02 in. (0.51 mm) and a ratio between the crack length and the disc radius a/R of about 0.3. A total of 12 CSTBD specimens were prepared with different values of the dip angle ψ of the planes of rock anisotropy ($\psi = 0°$, 45°, 90°), and with different values of the angle β between the crack and the loaded diameter. The test specimen characteristics are listed in Table 4. It is noteworthy that the crack initiation angle from a notch will in general differ from the one from a sharp crack. However, for a notch with a small tip radius ($r/a < 0.02$), this difference is negligible [55].

All specimens were brought to failure under a line load (Fig. 7) at a slow deformation rate of 0.02 in/min (0.51 mm/min.) by using a 100 kips (450 kN) MTS loading system. The testing requires only the recording of the maximum load; no load-displacement record was made during the testing. The procedure used to determine the fracture toughness of the shale in mode I (K_{IC}) and its fracture toughness in mode II (K_{IIC}) was as follows:

Table 6. Values of pure mode crack angles β_I and β_{II} for $\psi = 0°$, 45° and 90°

	$\psi = 0°$	$\psi = 45°$	$\psi = 90°$
β_I (deg.)	0	0.8	0
β_{II} (deg.)	28.2	27.6	25.9

Table 7. Measured failure load W_f and calculated values of K_{IC} and K_{IIC}

	Sample	β (deg.)	W_f (lb.)	F_I, F_{II}	K_{IC}, K_{IIC} (lb./in.$^{3/2}$)	Average (lb./in.$^{3/2}$)
$\psi = 0°$	SA1-1	0	549	$F_I = 1.156$	$K_{IC} = 500.3$	$K_{IC} = 568.3$
	SA1-2	0	726	$F_I = 1.167$	$K_{IC} = 636.4$	
	SA2-1	28.2	662	$F_{II} = -1.792$	$K_{IIC} = -805.7$	$K_{IIC} = -821.5$
	SA2-2	28.2	618	$F_{II} = -1.803$	$K_{IIC} = -837.3$	
$\psi = 45°$	SB1-1	0.8	707	$F_I = 1.089$	$K_{IC} = 557.8$	$K_{IC} = 495.5$
	SB1-2	0.8	509	$F_I = 1.090$	$K_{IC} = 433.2$	
	SB2-1	27.6	517	$F_{II} = -1.791$	$K_{IIC} = -639.3$	$K_{IIC} = -619.9$
	SB2-2	27.6	500	$F_{II} = -1.787$	$K_{IIC} = -600.5$	
$\psi = 90°$	SC1-1	0	723	$F_I = 1.031$	$K_{IC} = 467.6$	$K_{IC} = 542.0$
	SC1-2	0	664	$F_I = 1.039$	$K_{IC} = 456.0$	
	SC2-1	25.9	602	$F_{II} = -1.795$	$K_{IIC} = -749.7$	$K_{IIC} = -767.9$
	SC2-2	25.9	562	$F_{II} = -1.801$	$K_{IIC} = -717.2$	

(1 lb = 4.45 N; 1 in. = 25.4 mm)

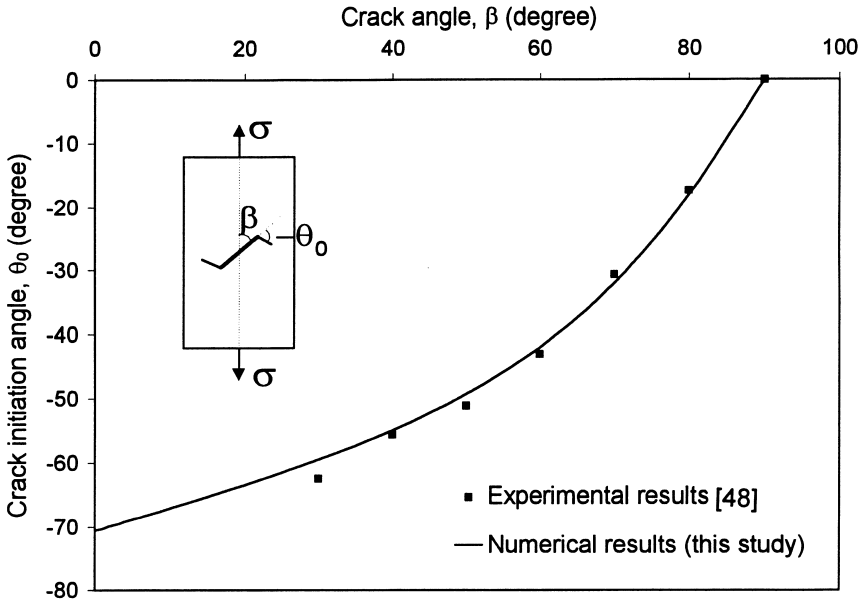

Fig. 20. Variation of crack initiation angle θ_0 with the crack angle β. Plexiglass plate subjected to uniaxial tension. Experimental results of Erdogan and Sih [48] and numerical predictions.

(1) Determine the elastic properties of the rock using Brazilian tests [42];

(2) Use the BEM to calculate the normalized SIFs (F_{I} and F_{II}). The input geometry (ψ, β, and a/R) should obviously be the same as that in the experiments;

(3) Conduct diametral loading of a CSTBD specimen with a certain crack angle β and record the failure load; and

(4) Calculate the fracture toughness using Equations (17) and (18).

After each Brazilian test, the direction of crack initiation and the path of crack propagation were recorded. These experimental observations were compared with numerical predictions as described in the following section.

Experimental results for pure mode I and mode II

The mode I fracture toughness and mode II fracture toughness of the shale were determined with the aforementioned procedure when the material inclination angle ψ was 0°, 45° and 90°. The shale was modeled as transversely isotropic with the plane of transverse isotropy parallel to the rock layers. The five elastic constants determined by diametral loading of uncracked discs [42] are listed in Table 5.

With the specimen geometry and the elastic constants of the shale known, a BEM analysis was con-

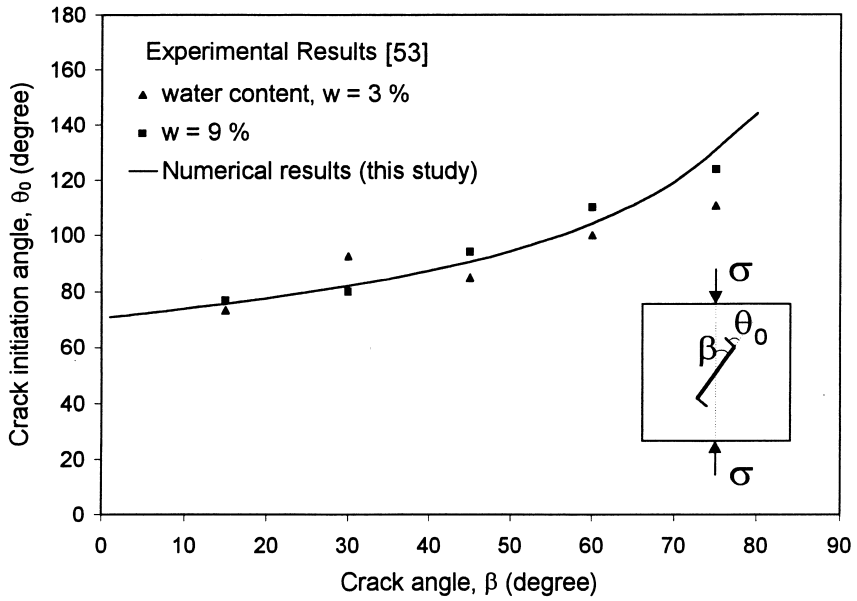

Fig. 21. Variation of crack initiation angle θ_0 with the crack angle β. Prismatic sample of kaolinite clay subjected to uniaxial compression. Experimental results of Vallejo [53] and numerical predictions.

Table 8. Comparison between crack initiation angles predicted numerically and observed experimentally in the tests on CSTBD specimens of shale

	Sample	β (deg.)	Experimental measurements (deg.)			Num. results (deg.)
			Tip-A	Tip-B	average	
$\psi = 0^\circ$	SA1-1	0	–1.0	0	–0.5	0
	SA1-2	0	–0.5	0	–0.3	0
	SA2-1	28.2	78.6	70.5	74.6	71.87
	SA2-2	28.2	79.0	76.4	77.7	71.78
$\psi = 45^\circ$	SB1-1	0.8	3.8	2.2	3.0	0.99
	SB1-2	0.8	3.5	7.0	5.3	1.06
	SB2-1	27.6	68.7	64.0	66.4	70.50
	SB2-2	27.6	67.8	73.5	70.7	70.46
$\psi = 90^\circ$	SC1-1	0	0	–3.8	–1.9	0
	SC1-2	0	2.0	0	1.0	0
	SC2-1	25.9	67.5	63.3	65.4	69.44
	SC2-2	25.9	70.9	62.2	66.6	69.49

Tip-A and Tip-B are defined in Fig. 7.

ducted to determine the variation of the normalized SIFs (F_I and F_{II}) with the angle β between the crack and the loading direction (see Fig. 7). The results of the BEM analysis are shown in Figs 17–19 when $\psi = 0^\circ$, 45° and 90°, respectively. These three figures can then be used to determine the angle β_I corresponding to pure mode I ($K_{II} = 0$) and the angle β_{II} corresponding to pure mode II ($K_I = 0$). The values of β_I and β_{II} for $\psi = 0^\circ$, 45° and 90° are listed in Table 6.

From the failure loads recorded by laboratory testing of discs oriented with an initial crack inclined at β_I or β_{II}, the critical SIF or fracture toughness in mode I (K_{IC}) and that in mode II (K_{IIC}) could be determined. The values of the failure load W_f and the fracture toughness for the shale are reported in Table 7 when $\psi = 0^\circ$, 45° and 90°. The negative sign of K_{IIC} in Table 7 is associated with the adopted sign convention of the mode II SIF (see Fig. 4).

CRACK INITIATION ANGLES AND PROPAGATION PATHS

Comparison of numerical predictions of crack initiation angles with experimental results

In order to check the validity of our crack prediction procedure, the tests of Erdogan and Sih [48] were reproduced numerically with our new BEM formulation. Erdogan and Sih conducted uniaxial tension tests on isotropic Plexiglass sheets $9 \times 18 \times 0.188$ in. ($229 \times 457 \times 4.8$ mm) in size containing a 2 in. (50.8 mm) long central crack. The crack orientation angle β between the crack plane and the tensile stress was varied. Figure 20 shows the variation of the crack initiation angle θ_0 with the crack angle β determined numerically and experimentally. A good agreement is found between the experimental results of Erdogan and Sih [48] and our numerical predictions.

Another verification was done using the experimental results of Vallejo [53]. The latter conducted uniaxial compression tests on cracked prismatic specimens of kaolonite clay $3 \times 3 \times 1$ in. ($76.2 \times 76.2 \times 25.4$ mm) in

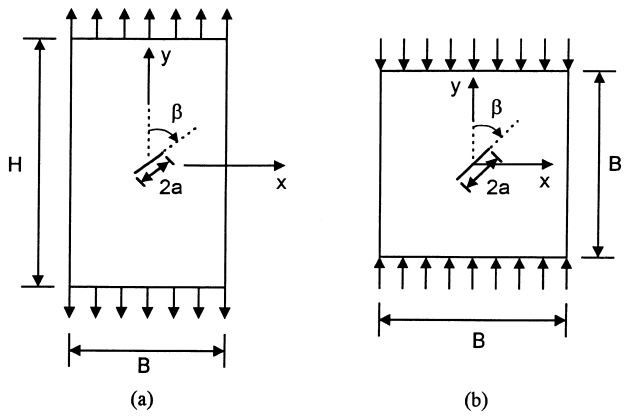

Fig. 22. Mixed mode cracking problem. (a) Rectangular plate with a central inclined crack subjected to uniaxial tension, (b) square plate with a central inclined crack subjected to uniaxial compression.

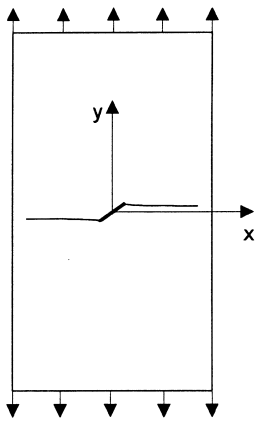

Fig. 23. Numerical simulation of crack propagation ($\beta = 43^\circ$). Plate of titanium subjected to uniaxial tension.

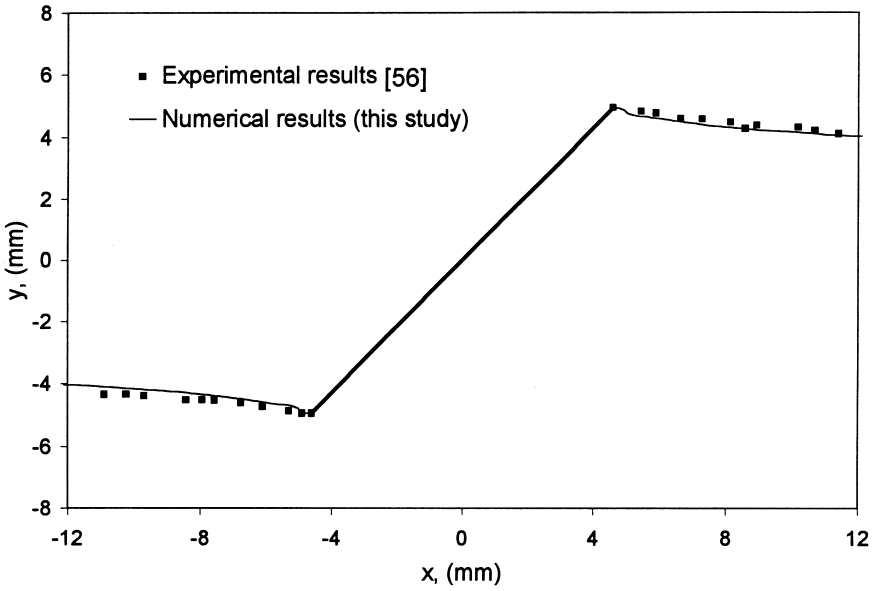

Fig. 24. Propagation of a crack at the center of a plate of titanium under uniaxial tension. Comparison between experimental results of Pustejovsky [56] and numerical predictions.

size containing a central crack 0.98 in. (24.9 mm) in length. Several tests were carried out by varying the crack angle β between the crack plane and the compressive stress. Figure 21 shows a comparison between the crack initiation angles measured experimentally and those predicted numerically. Again, a good agreement is found between the two approaches.

Our crack prediction procedure was then used to predict the crack initiation angles in the diametral compression tests of CSTBD specimens of shale for the three values of the inclination angle $\psi = 0°$, $45°$ and $90°$ considered in the tests. Table 8 gives a comparison between the crack initiation angles measured experimentally and those predicted numerically with the BEM method. Good agreement is found between the two sets of crack initiation angles. It can be seen that our numerical procedure based on the BEM can predict well the crack initiation angle in cracked discs of anisotropic rocks under diametral loading.

Comparison of numerical predictions of crack propagation paths with experimental results

In order to check the validity of the proposed BEM for predicting the crack propagation paths, both isotropic rectangular and square plates with a central inclined crack subjected to uniaxial tension and com-

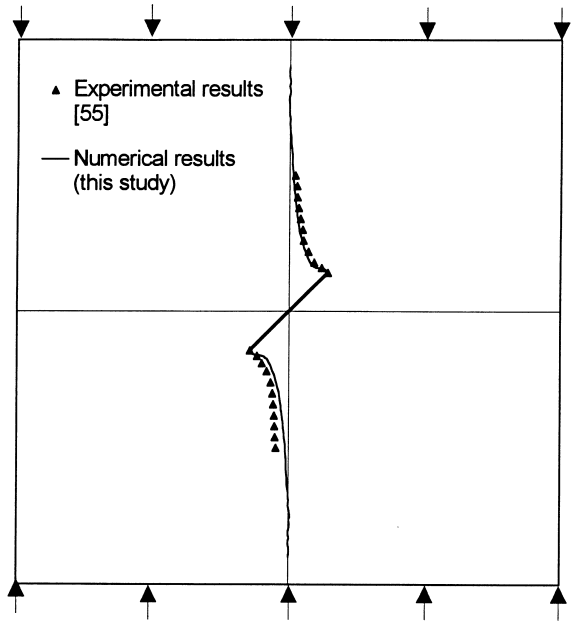

Fig. 25. Propagation of a crack at the center of a plate of granite subjected to uniaxial compression. Comparison between experimental results of Ingraffea [55] and numerical predictions.

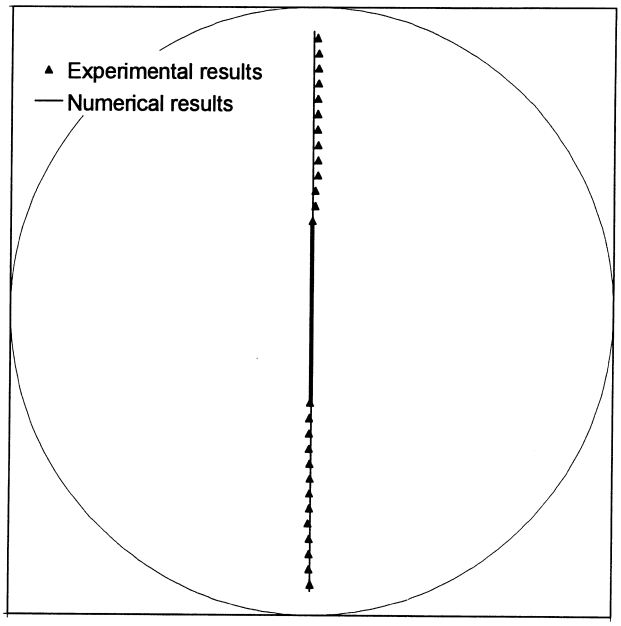

Fig. 26. Propagation of a crack at the center of a CSTBD specimen with $\psi = 0°$ and $\beta = 0°$. Comparison between experimental observations and numerical predictions for specimen SA1-1.

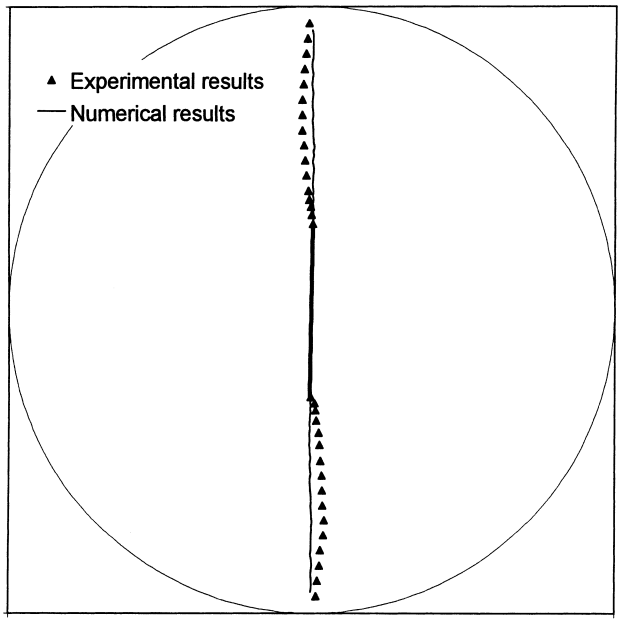

Fig. 27. Propagation of a crack at the center of a CSTBD specimen with $\psi = 45^\circ$ and $\beta = 0.8^\circ$. Comparison between experimental observations and numerical predictions for specimen SB1-2.

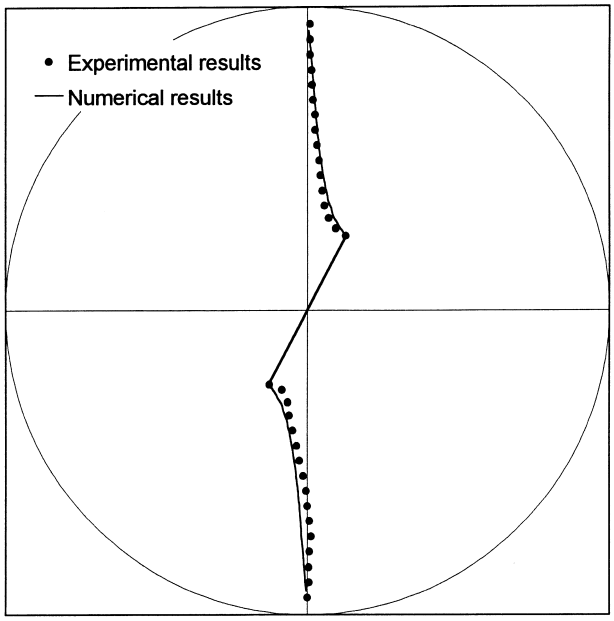

Fig. 29. Propagation of a crack at the center of a CSTBD specimen with $\psi = 0^\circ$ and $\beta = 28.2^\circ$. Comparison between experimental observations and numerical predictions for specimen SA2-1.

pression are considered [see Fig. 22(a) and (b)]. These mixed-mode cracking problems have been studied experimentally by Ingraffea [55] and Pustejovsky [56]. Comparison of crack propagation paths by the proposed BEM with the experimental results is discussed in this section.

Experimental measurements of crack growth in an isotropic titanium Ti–6Al–4V plate were made by Pustejovsky [56]. In these experiments, a crack initially inclined with respect to the applied stress was allowed to grow under tensile loading [see Fig. 22(a)]. The reported material properties of the specimens were $E = 16 \times 10^6$ psi (112 GPa), $v = 0.29$, and the ultimate tensile strength $T_u = 135$ ksi (945 MPa). The specimens were $3 \times 8 \times 1/8$ in. ($76.2 \times 203.2 \times 3.2$ mm) in size and were cut using a carbide cutoff-wheel to give a initial crack length $2a = 0.53$ in (13.5 mm). One of the test specimens (defined as specimen CSG-04) had a crack angle $\beta = 43^\circ$. A numerical simulation of crack propagation paths in that specimen was conducted with the BEM using 32 continuous quadratic elements for the outer boundary and 10 initial discontinuous elements

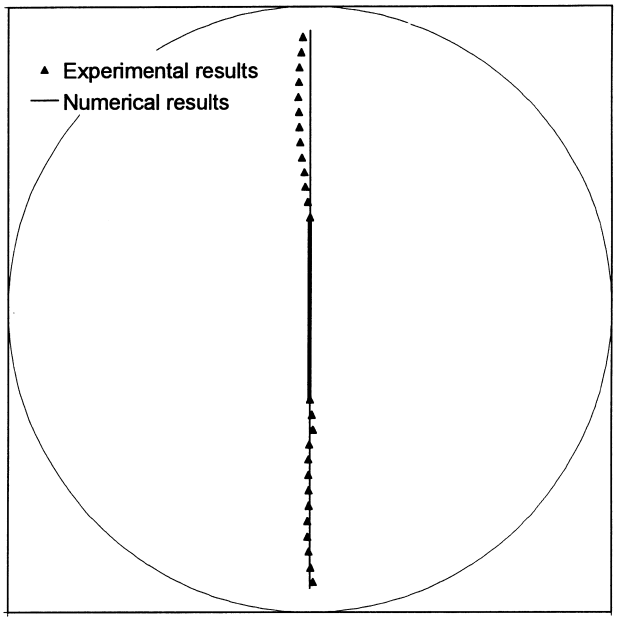

Fig. 28. Propagation of a crack at the center of a CSTBD specimen with $\psi = 90^\circ$ and $\beta = 0^\circ$. Comparison between experimental observations and numerical predictions for specimen SC1-1.

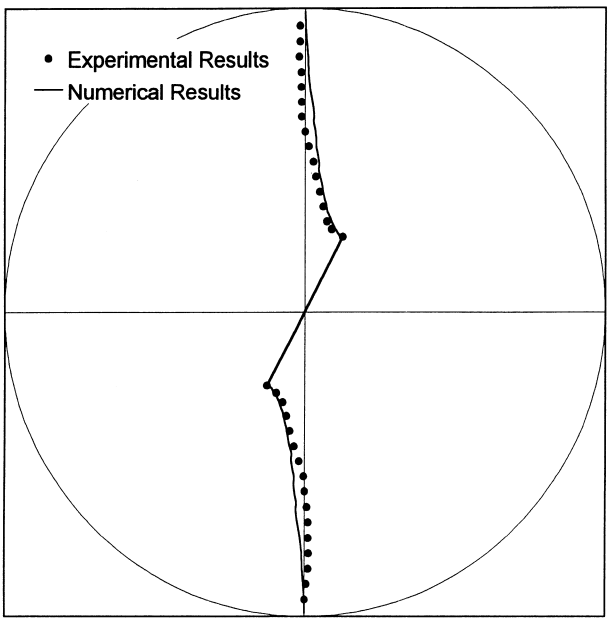

Fig. 30. Propagation of a crack at the center of a CSTBD specimen with $\psi = 45^\circ$ and $\beta = 27.6^\circ$. Comparison between experimental observations and numerical predictions for specimen SB2-2.

for the crack boundary. The result of the numerical simulation is shown in Fig. 23. It is noted that the subsequent crack path is slightly curved and nearly perpendicular to the applied load. This observation is consistent with the results of Yan and Nguyen-Dang [39] using the dual BEM. Comparison of simulated crack propagation paths with the experimental observations of Pustejovsky [56] in the vicinity of the crack tip is shown in Fig. 24. A good agreement is found between the experimental results and the numerical prediction.

Another numerical simulation of crack propagation was made for a square sheet with a central inclined crack under uniaxial compression with the geometry of Fig. 22(b). Ingraffea [55] conducted compression tests on initially cracked granite specimens $4 \times 4 \times 0.75$ in. ($101.6 \times 101.6 \times 19.1$ in) in size containing an initial crack with a length of 0.4 in. (10.2 mm). The crack angle β was fixed at 45°. The mechanical properties of the granite were $E = 9.01 \times 10^6$ psi (63 GPa), $\nu = 0.243$, and its ultimate compression strength was $q_u = 38{,}500$ psi (269 MPa). The crack propagation path was simulated using the BEM with 20 continuous elements on the outer boundary and 10 initial discontinuous elements on the crack boundary. Figure 25 shows a comparison between the crack propagation path observed experimentally and that simulated numerically. Again, a good agreement is found between these two approaches.

In order to verify further the validity of the BEM procedure for cracked anisotropic materials, the crack propagation path in the CSTBD specimens of shale was numerically predicted and compared with the actual laboratory observations. Details of specimen dimensions, testing procedure, crack geometry, and photographs after failure can be found in the doctoral thesis of Chen [57]. All crack propagation paths tend to be parallel to the loading direction and to approach the loading points. The BEM was also used to simulate crack propagation in the CSTBD specimens. The outer boundary and crack surface were discretized with 28 continuous and 20 initial discontinuous quadratic elements, respectively. Figures 26–31 show the observed and predicted crack propagation paths for specimens SA1-1, SB1-2, SC1-1, SA2-1, SB2-2, and SC2-1, respectively. Good agreement is found between the two approaches. It is therefore concluded that the proposed BEM procedure can simulate well the angles occurring in the process of crack propagation for both isotropic and anisotropic materials.

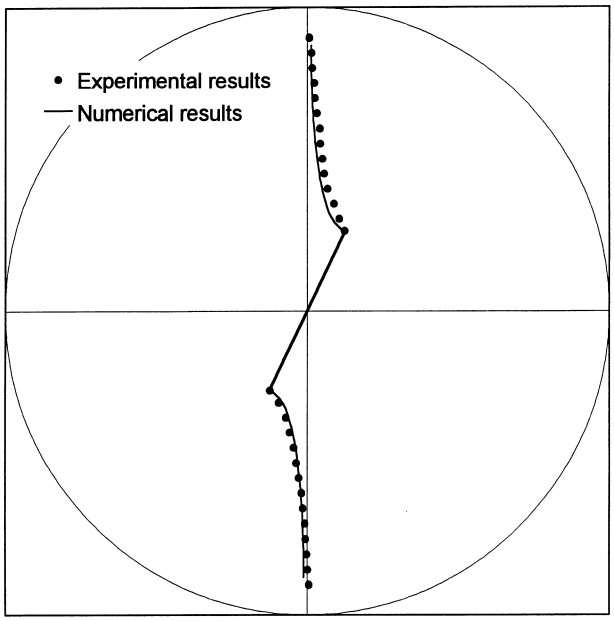

Fig. 31. Propagation of a crack at the center of a CSTBD specimen with $\psi = 90°$ and $\beta = 25.9°$. Comparison between experimental observations and numerical predictions for specimen SC2-1.

CONCLUSIONS

This paper shows that the mixed mode stress intensity factors of anisotropic rocks under diametral loading can be successfully determined by the BEM. The effect of crack length, crack angle, anisotropic orientation and degree of material anisotropy on the values of SIFs was also discussed. Thus, rock fracture toughness can be computed by diametral loading of Cracked Straight Through Brazilian Disc (CSTBD) specimens. This was demonstrated by testing CSTBD specimens of a shale under pure mode I and mode II loading with rock layers inclined at $\psi = 0°$, 45° and 90° from the horizontal.

A new BEM procedure based on the maximum tensile stress failure criterion was developed to predict the crack initiation direction and the crack propagation path in anisotropic rock discs under mixed mode loading. A good agreement was found between crack initiation angles and propagation paths predicted with the BEM and experimental observations reported by previous researchers on isotropic materials. Numerical simulations of crack initiation and propagation in the CSTBD specimens of a shale were also found to compare well with the experimental results. It is concluded that, in general, the fracture toughness of anisotropic rocks depends on the rock properties and the orientation of the crack direction.

Accepted for publication 8 November 1997

Acknowledgements—This research is funded in part by National Science Foundation, under grants MS-9215397 and CMS-9622645.

REFERENCES

1. Griffith, A. A., The phenomena of rupture and flow in solids. *Phil. Trans. R. Soc. London, Series A*, 1920, **221,** 163–198.
2. Irwin, G. R., Analysis of stresses and strains near the end of a crack. *J. Appl. Mech.*, 1957, **24,** 361–364.
3. Libatskii, L. L. and Kovchik, S. E., Fracture of discs containing cracks. *Sov. Mater. Sci.*, 1967, **3,** 334–339.
4. Rooke, D. P. and Tweed, J., The stress intensity factors of a radial crack in a point loaded disc. *Int. J. Eng. Sci.*, 1973, **11,** 285–290.

5. Isida, M., Arbitrary loading problems of doubly symmetric regions containing a central crack. *Eng. Fracture Mech.*, 1975, **7,** 505–514.
6. Murakami, Y., A simple procedure for the accurate determination of stress intensity factors by finite element method. *Eng. Fracture Mech.*, 1976, **8,** 643–655.
7. Guo, H., Aziz, N. I. and Schmidt, L. C., Rock fracture-toughness determination by the Brazilian test. *Eng. Geol.*, 1993, **33,** 177–188.
8. Awaji, H. and Sato, E., Combined mode fracture toughness measurement by the disk test. *J. Eng. Mater. Technol.*, 1978, **100,** 175–182.
9. Atkinson, C., Smelser, R. E. and Sanchez, J., Combined mode fracture via the cracked Brazilian disk test. *Int. J. Fracture*, 1982, **18,** 279–291.
10. Fowell, R. J. and Xu, C., The use of the cracked Brazilian disc geometry for rock fracture investigations. *Int. J. Rock Mech. Min. Sci. Geomech. Abstr.*, 1994, **31,** 571–579.
11. Chen, C. S., Pan, E. and Amadei, B., Analysis of stress intensity factors and stress distribution for cracked discs of anisotropic rock under diametral loading. *Proc. 19th. Conf. Theor. Appl. Mech. Taiwan*, 1995, **3,** 297–303.
12. Schmidt, R. A., Fracture-toughness testing of limestone. *Exp. Mech.*, 1976, **16,** 161–167.
13. Schmidt, R. A. and Huddle, C. W., Effect of confining pressure on fracture toughness of Indiana limestone. *Int. J. Rock Mech. Min. Sci. Geomech. Abstr.*, 1977, **14,** 289–293.
14. Ingraffea, A. R. and Schmidt, R. A., Experimental verification of a fracture mechanics model for tensile strength prediction of Indiana limestone. *Proc. 19th U.S. Symp. Rock Mech.*, University of Nevada, 1978, pp. 247–253.
15. Costin, L. S., Static and dynamic fracture behavior of oil shale. *Fracture Mechanics for Ceramics, Rocks, and Concrete, ASTM STP 745*. American Society for Testing and Materials, 1981, pp. 169–184.
16. Huang, J. A., An experimental investigation concerning the comprehensive fracture toughness of some brittle rocks. *Int. J. Rock Mech. Min. Sci. Geomech. Abstr.*, 1985, **22,** 99–104.
17. Ouchterlony, F. (Co-ordinator), Suggested methods for determining the fracture toughness of rock. *Int. J. Rock Mech. Min. Sci. Geomech. Abstr.*, 1988, **25**, 71–96.
18. Ingraffea, A. R., Gunsallus, K. L., Beech, J. F. and Nelson, P. P., A short-rod based system for fracture toughness testing of rock. *Chevron-Notched Specimens: Testing and Stress Analysis, ASTM STP 855*. American Society for Testing and Materials, 1984, pp. 152–166.
19. Swan, G. and Alm, O., Sub-critical crack growth in Stripa granite: Direct observations. *Proc. 23rd U.S. Symp. Rock Mech.*, University of California, Berkeley, 1982, pp. 542–550.
20. Sun, Z. and Ouchterlony, F., Fracture toughness of Stripa granite cores. *Int. J. Rock Mech. Min. Sci. Geomech. Abstr.*, 1986, **23,** 399–409.
21. Senseny, P. E. and Pfeifle, T. W., Fracture toughness of sandstones and shales. *Proc. 25th U.S. Symp. Rock Mech.*, Northwestern University, 1984, pp. 390–397.
22. Gunsallus, K. L. and Kulhawy, F. H., A comparative evaluation of rock strength measures. *Int. J. Rock Mech. Min. Sci. Geomech. Abstr.*, 1984, **21,** 233–248.
23. Ouchterlony, F., A presentation of the ISRM suggested methods for determining fracture toughness of rock materials. *Proc. 6th ISRM Congr., Montreal*, Vol. 2. Balkema, Rotterdam, 1987, pp. 1181–1186.
24. Shetty, D. K., Rosenfield, A. R. and Duckworth, W. H., Fracture toughness of ceramics measured by a chevron-notched diametral compression test. *J. Am. Ceram. Soc.*, 1985, **68,** c325–c443.
25. Fowell, R. J. (Co-ordinator), Suggested methods for determining mode I fracture toughness using cracked chevron notched Brazilian disc. *Int. J. Rock Mech. Min. Sci. and Geomech. Abstr.*, 1995, **32**, 57–64.
26. Sanchez, J., *Application of the Disk Test to Mode I–II Fracture Analysis*. M.S. thesis, Department of Mechanical Engineering, University of Pittsburgh, 1979.
27. Shetty, D. K., Rosenfield, A. R. and Duckworth, W. H., Mixed-mode fracture of ceramic in diametral compression. *J. Am. Ceram. Soc.*, 1986, **69,** 437–443.
28. Hirose, S., Taniguchi, T., Ouchterlony, F. and Nakagawa, K., The effect of anisotropy on the K_I calibration of ISRM standard fracture toughness. *Int. IRSM Congr. Rock Mech.*, 1995, **1,** 165–168.
29. Shephard, M. S., Yehia, N. A. B., Burd, G. S. and Weidner, T. J., Automatic crack propagation traction. *Comput. Struct.*, 1985, **20,** 211–223.
30. Boone, T. J., Wawrzynek, P. A. and Ingraffea, A. R., Finite element modelling of fracture propagation in orthotropic materials. *Eng. Fracture Mech.*, 1987, **26,** 185–201.
31. Wawrzynek, P. A., Martha, L. F. and Ingraffea, A. R., A computational environment for the simulation of fracture processes in three dimensions. In *Anal. Numer. Exper. Aspects of Three-dimensional Fracture Process*, ed. A. J. Rosakis *et al.* ASME, AMD-91, 1988, pp. 321–327.
32. Swenson, D. V. and Ingraffea, A. R., Modelling mixed-mode dynamic crack propagation using finite elements: Theory and applications. *Comput. Mech.*, 1988, **3,** 381–397.
33. Wei, K. and De Bremaecker, J. -C., Fracture growth under compression. *J. Geoph. Res.*, 1994, **99**(B7), 13781–13790.
34. Sollero, P., Aliabadi, M. H. and Rooke, D. P., Anisotropic analysis of cracks emanating from circular holes in composite laminates using the boundary element method. *Eng. Fracture Mech.*, 1994, **49**(B7), 213–224.
35. Shen, B. and Stephansson, O., Modification of the G-criterion for crack propagation subjected to compression. *Eng. Fracture Mech.*, 1994, **47**(B7), 177–189.
36. Scavia, C., A method for the study of crack propagation in rock structures. *Geotechnique*, 1995, **45**(B7), 447–463.
37. Portela, A., Aliabadi, M. H. and Rooke, D. P., Dual boundary element incremental analysis of crack propagation. *Comput. Struct.*, 1993, **46**(B7), 237–247.
38. Prasad, N. N. V. and Aliabadi, M. H., Incremental crack growth in thermoelastic problems. *Int. J. Fracture*, 1994, **66**(B7), R45–R50.
39. Yan, A. M. and Nguyen-Dang, H., Multiple-cracked fatigue crack growth by BEM. *Comput. Mech.*, 1995, **16**(B7), 273–280.
40. Pan, E. and Amadei, B., Fracture mechanics analysis of 2D anisotropic media with a new boundary element method. *Int. J. Fracture*, 1996, **77**(B7), 161–174.
41. Lekhnitskii, S. G., *Anisotropic Plates*, translated by S. W. Tsai. Gordon and Breath, 1957.
42. Chen, C. S., Pan, E. and Amadei, B., Determination of deformability and tensile strength of anisotropic rock using Brazilian tests. *Int. J. Rock Mech. Min. Sci. and Geomech. Abstr.*, 1997, submitted.
43. Sih, G. C., Paris, P. C. and Irwin, G. R., On cracks in rectilinearly anisotropic bodies. *Int. J. Fracture*, 1965, **3**(B7), 189–203.
44. Cerrolaza, M. and Alarcon, E., A bi-cubic transformation for the numerical evaluation of the Cauchy principal value integrals in boundary methods. *Int. J. Num. Methods Eng.*, 1989, **28**(B7), 987–999.
45. Sollero, P. and Aliabadi, M. H., Fracture mechanics analysis of anisotropic plates by the boundary element method. *Int. J. Fracture*, 1993, **64**(B7), 269–284.
46. Rice, J. R., A path independent integral and the approximate analysis of strain concentration by notches and cracks. *Trans. ASME J. Appl. Mech.*, 1968, **35**(B7), 379–386.
47. Chu, S. J. and Hong, C. S., Application of the J_k integral to mixed mode crack problems for anisotropic composite laminates. *Eng. Fracture Mech.*, 1990, **35**(B7), 1093–1103.
48. Erdogan, F. and Sih, G. C., On the crack extension in plates under plane loading and transverse shear. *J. Basic Eng.*, 1963, **85**(B7), 519–527.
49. Palaniswamy, K. and Knauss, W. G., Propagation of a crack under general, in-plane tension. *Int. J. Fracture*, 1972, **8**(B7), 114–117.
50. Sih, G. C., Strain-energy density factor applied to mixed mode crack problems. *Int. J. Fracture*, 1974, **10**(B7), 305–321.
51. Woo, C. W. and Ling, H. L., On angle crack initiation under biaxial loading. *J. Strain Anal.*, 1984, **19**(B7), 51–59.
52. Richard, H. A., Examination of brittle fracture criteria for overlapping mode I and mode II loading applied to cracks. In *Application of Fracture Mechanics to Materials and Structures*, ed. G. C. Sih *et al.* Martinus Nijhoff Pub., The Hague, 1984, pp. 309–316.
53. Vallejo, L. E., The brittle and ductile behavior of a material containing a crack under mixed-mode loading. *Proc. 28th U.S. Symp. Rock Mech.*, University of Arizona, Tucson, 1987, pp. 383–390..

54. Whittaker, B. N., Singh, R. N. and Sun, G., *Rock Fracture Mechanics: Principles, Design and Applications*. Elsevier, New York, 1992.
55. Ingraffea, A. R., Discrete Fracture Propagation in Rock Laboratory Tests and Finite Element Analysis. Ph.D. thesis, Department of Civil Eng., University of Colorado, 1977.
56. Pustejovsky, M. A., Fatigue crack propagation in titanium under general in-plane loading — I: Experiments. *Eng. Fracture Mech.*, 1979, **11**(B7), 9–15.
57. Chen, C. S., Characterization of deformability, strength, and fracturing of anisotropic rocks using Brazilian tests. Ph.D. thesis, Department of Civil Eng., University of Colorado, 1996.

APPENDIX A

Green's Functions

For concentrated point forces acting at z_k^0 ($z_k^0 = x^0 + \mu_k y^0$) in an infinite plate, the Green's tractions, T_{ij}, and displacements, U_{ij}, are equal to [45]

$$T_{ij}(z_k, z_k^0) = 2\mathrm{Re}\big[Q_{j1}(\mu_1 n_x - n_y)A_{i1}/(z_1 - z_1^0) + Q_{j2}(\mu_2 n_x - n_y)A_{i2}/(z_2 - z_2^0)\big] \tag{A.1}$$

and

$$U_{ij}(z_k, z_k^0) = 2\mathrm{Re}\big[P_{j1}A_{i1}\ln(z_1 - z_1^0) + P_{j2}A_{i2}\ln(z_2 - z_2^0)\big] \quad (i, j = 1, 2). \tag{A.2}$$

In Equations (A.1) and (A.2), n_x and n_y are the outward normal vectors of the field point, and $Q_{11} = \mu_1$, $Q_{12} = \mu_2$, and $Q_{21} = Q_{22} = -1$. The complex coefficients A_{jk} are solutions of the following equation

$$\begin{bmatrix} 1 & -1 & 1 & -1 \\ \mu_1 & -\overline{\mu}_1 & \mu_2 & -\overline{\mu}_2 \\ P_{11} & -\overline{P}_{11} & P_{12} & -\overline{P}_{12} \\ P_{21} & -\overline{P}_{21} & P_{22} & -\overline{P}_{22} \end{bmatrix} \begin{bmatrix} A_{j1} \\ \overline{A}_{j1} \\ A_{j2} \\ \overline{A}_{j2} \end{bmatrix} = \begin{bmatrix} \delta_{j2}/(2\pi i) \\ -\delta_{j1}/(2\pi i) \\ 0 \\ 0 \end{bmatrix} \tag{A.3}$$

where δ_{jk} is the Kronecker's delta.